Histomorphometric Analysis of Structural and Bone Remodeling Parameters in the Underloaded Ovine Calcaneus

Max Lister MPhil Thesis

Date Submitted:

Supervised by: Dr. Jon Power

and

Dr. Stephen Fôn Hughes

Thesis submission for Master of Philosophy

(MPhil)

i) Declaration

This is to certify that the work submitted in this thesis is my own and has not been submitted for any other degree

Signed: ……

ii) Acknowledgements

Firstly I would like to thank my supervisors, Dr Jon Power and Dr Stephen Fôn Hughes whom without I would not have had the opportunity to carry out this thesis. As my supervisors, they have provided me with an incredible amount of help and support of which I could not be more grateful. Secondly, I would like to give my thanks to my parents for funding me and supporting me throughout, without them I would not have been able to continue learning after my undergraduate degree. Finally, I would like to thank all my friends who supported me throughout my thesis, specifically Mabon and Amy for keeping me well fed and rested. This would not have been possible without you.

iii) Abstract

Osteoporosis is a disease that affects over three million people in the UK (NHS, 2016), and is categorized by a reduced bone mass leading to decreased bone strength and increased fragility. Clinical features of osteoporotic fractures include increased morbidity (physical impairment, reduced quality of life, pain), greater risk of new fractures and increased mortality (Geusens, 2008).

During the lifetime of a typical human, bones are their strongest whilst a person is in their early-mid 20's. As one ages bone loss begins to occur around the age of 35. One important causal factor leading to osteoporosis is lack of weight-bearing physical activity, which might impact the elderly human population at sites such as the femoral neck resulting in fragility fractures. Around 70,000-75,000 hip fractures occur in the UK each year, additionally every year an increase in incident rates has been observed partly due to an aging population (NHS, 2016).

The relationship between a decreased mechanical load and resulting in reduced bone mass is well established. The structural and cellular consequences of mechanical underloading within a temporal animal model are yet to be fully explored.

The objective of the current study was to determine the temporal structural changes occurring due to the influence of mechanical under-loading (experienced at day 0/baseline, week 4 and week 16) within an ovine skeletal model. Additionally, this experimental system provided insight into the cellular activity (in terms of bone remodeling) associated with a reduced mechanical loading environment.

Within this model by week 16 of mechanical under-loading, an increase in cortical porosity (4%, p=0.017) within the dorsal region and reduced cortical thickness (19.7%, p=0.025) across all combined regions (as well as a regional decrease of 15% and 23% within the medial and ventral regions respectively) was observed.

These changes indicating a reduction in bone mass were accompanied by increased cortical remodeling medially (58%;p=0.028) as evidenced by an increase in the proportion (%) of canals undergoing bone formation within that anatomical region.

These data demonstrate a reduction in bone mass and increased bone remodeling associated with reduced mechanical load within this skeletal site. Additionally, the data presented here of decreased mechanical load appear to support the observed bone loss and elevated remodeling occurring within the osteoporotic human femoral neck. This investigation,therefore, validates the underloaded ovine calcaneus as a suitable experimental model to investigate the possible pathological events associated with disuse osteoporosis.

Contents

Abbreviations

Acid phosphatase 5 (ACP5)

Arbeitsgemeinschaft für Osteosynthesefragen (AO): A nonprofit organization that provides surgical equipment e.g. bone fixators.

Basic multicellular unit (BMU)

Bone mass content (BMC)

Bone mineral density (BMD)

Ethylenediaminetetraacetic acid (EDTA)

High-resolution peripheral quantitative computed tomography (HR-pQCT)

Immunohistochemical (IHC)

Insulin growth factor-I (IGF-I)

Interleukin- 1β (IL-1β)

Interleukin-6 (IL-6)

Micro-computed Tomography (μCT)

Neutral axis (NA)

Osteoprotegerin (OPG)

OPG ligand (OPGL)

Parathyroid hormone (PTH)

Receptor activator nuclear factor kappa-B (RANK)

Receptor activator nuclear factor kappa-B ligand (RANKL)

Reverse transcription polymerase chain reaction (RT-PCR)

Sodium hydroxide (NaOH)

Standard error (SE)

Synchrotron radiation micro-computed tomography (SRμCT)

Tartrate-resistant acid phosphatase (TRAP)

Tumour necrosis factor-α (TNF- α)

Chapter 1.1: The Structure of Bone and cellular components

1.1.1: Skeletal and Bone Physiology

The skeleton serves five major functions, as a support system for its surrounding tissues for example nerves, blood, fat, and skin; as a method of protection for vital organs such as lungs, heart and the brain; to aid with body movement through the use of bones as levers pulled on by muscles attached to other bone and finally it manufactures blood cells within red bone marrow (Rizzo, 2015). Red bone marrow is called as such because of the red colour it expresses and its active haematopoietic tissue. The creation of blood cells within red bone marrow derives from the large undifferentiated stems cells found inside (Khurana, 2014).

Within the human skeleton, there are 206 major bones, these can be grouped into six general categories (Martini, Nath, & Bartholomew, 2014):

- Sutural bones – flat, small, unevenly shaped bones that reside between the flat bones of the skull.
- Sesamoid bones – these small, flat bones have a unique and varied location within the body (at least 26 different locations) and account for the variation in bone count between subjects.

- Irregular bones – bones with a complex shape
- Flat bones – slender and flat in shape
- Short bones – small and box-like, having roughly equal dimensions.
- Long bones – extended, consisting of a shaft (diaphysis) with two ends (epiphyses) of greater width than the shaft.

The grouping of bones into these categories allows for an easier diagnosis or treatment of the affected area. For example, Ewing sarcoma typically occurs in the long and flat bones of Caucasian males under 20 (Britannica, 2012). Another example would be Monostotic fibrous dysplasia which causes unusual bone growth and deformity in the flat and sutural bones of the skull as well as the long bones of the limbs (Collins, 2015).The macroscopic bone structure is categorised into two major arrangements the cortical bone and the cancellous (trabecular/spongey) bone. The honeycombed structure of trabecular bone accounts for around 20% of the total bone mass and can be seen at the end of long bones such as the femur (Figure 1). Comprising of around 85% of the whole skeleton, cortical bone is found primarily in the shafts of long bones and on the surfaces of flat bones, concentrated around the Haversian canals. Contained within these Haversian canals are blood vessels and nerve fibers that allow communication between osteocytes. A Haversian system or osteon consists

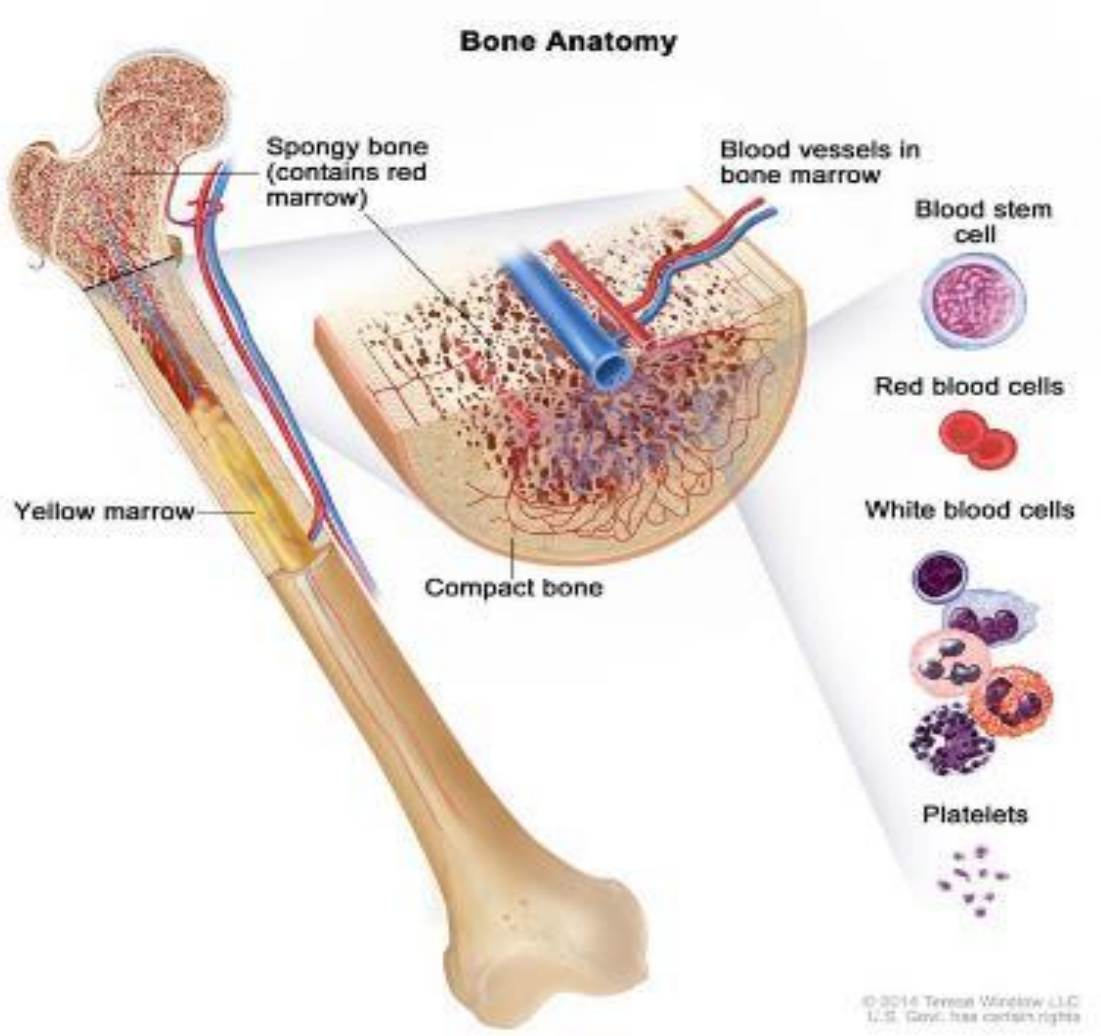

Figure 1: The physiology of long bone. (Childhood Acute Myeloid Leukemia/Other Myeloid Malignancies Treatment (PDQ®)–Patient Version, 2016)

of the Haversian canal, lamellae, canaliculi, and osteocytes. The osteon is the primary functional unit of cortical bone (Christiansen, 2001).

Bone is a highly specialized connective tissue composite formed of two different phases. The mineral phase mainly contains hydroxyapatite crystals deposited in the collagen fibers (Weiner, 1986), whereas the organic phase consists purely of type I collagen

fibers with bone matrix cells. These two phases provide a structural support system with mechanisms by which bone dynamically changes shape and size compensating for any variations in mechanical forces and loads. The mineral phase specifically reacts to the change in load due to its greater tensile strength, which allows for fracture energy to dissipate easier within protein increasing the overall toughness of the bone (Baohua & Huajian, 2004). During the course of an adult's life bone tissue is repeatedly remodeled, this allows for the repair of fatigue damage caused by continually changing mechanical and physiological factors. For example bone loss is commonly seen in aging patients, Young et al,. (2015) observed in patients between the ages of 32 and 56 further adaptation of preferential orientation under hip joint load, as well as a thickening of the trabecular under the loading path and a weakening of it out of the loading path. This preference of bone formation around the loading zone leads to an overall reduction in bone mass and an increased risk of fracture.

1.1.2: Cellular Components of Bone

The cellular structure of bone is formed by four equally important cells (Florencio-Silva, da Silva Sasso, Sasso-Cerri, Simões, & Cerri, 2015): Osteocytes, comprise of up to 95% of total bone cells and react to mechanical stimuli through the production of biochemical markers. Osteoblasts, located along the bone surface these cells account for 4-6% of total resident bone cells and

function as bone forming units. Osteoclasts, large multinucleated cells originating from mononuclear cells of the hematopoietic stem cell lineage whose primary function is bone resorption. Bone Lining Cells, covering the surface of bone these quiescent flat osteoblasts exhibit neither resorption or bone formation. Instead they prevent direct interaction between osteoclasts and the bone matrix, in addition, they're vital to osteoclast differentiaton, producing osteoprotegerin (OPG) and receptor activator nuclear factor kappa-B ligand (RANKL).

The most commonly found cell within mature bone tissue; osteocytes can be located within the lacunae and canaliculi of the

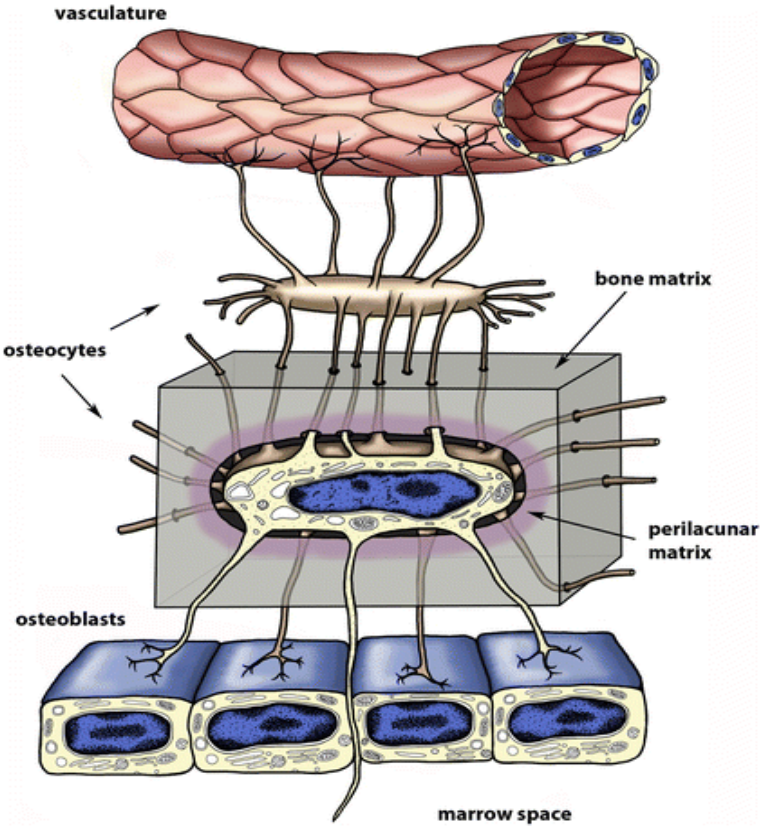

Figure 2: Schematic representation of an osteocyte embedded contained by the bone matrix within its lacuna. (Dallas, Prideaux, & Bonewald, 2013)

bone. Long channels of the canaliculi within the bone matrix allow for the passing of nutrients and oxygen from blood vessels to osteocytes, these channels can also be used for trafficking molecules between cells (Figure 2). Consequently, independent cells from deep within the bone matrix to surface cells can communicate with each other without the need for direct contact (Klein-Nulend, Bacabac, & Mullender, 2005). In addition, osteocyte dendrites have been found to possess a mechanism by which they increase the acidity of their microenvironment, dissolving mineral. Un-moderated demineralisation could lead to bone loss and therefore low bone mass typically found within bone-loss related diseases such as osteoporosis (Nobuhito, et al., 2016). The changes in bone mass found in such conditions are controlled by the continuous cycle of remodeling. Bone remodeling comprises four separate stages (Rucci, 2008);

1. Activation: This is where mechanical loading is sensed by osteocytes beginning a signalling cascade of several osteocyte derived factors (e.g. insulin growth factor-I (IGF-I) (Lean, Mackay, Chow, & Chambers, 1996), tumour necrosis factor-α (TNF-α) (Katsuyama, et al., 2015), parathyroid hormone (PTH) (Jilka, et al., 1999) and interleukin-6 (IL-6) (Tamura, et al., 1993)) from different sources into the surrounding micro-environment activating the quiescent osteoblasts and subsequent cells.

2. Differentiation: Multinucleated osteoclasts differentiate, resorbing old bone.

3. Reversal: The appearance of mononuclear cells on the surface of the bone.

4. Formation: Wherein osteoblasts produce new bone, completely replacing resorbed bone.

Osteoblasts can be found on all bone surfaces, predominantly on periosteum, canal and trabecular surfaces when undergoing bone formation (Hadjidakis & Androulakis, 2006).Disuse and under-loading of bone have an effect on the balance of the bone formation and resorption stages of remodeling, specifically an increase in bone resorption and a decrease in formation leading to an overall net loss of bone and a higher porosity (Weinreb, Rodan, & Thompson, 1989). Within the underloaded human model of Spaceflight-induced bone loss, bone resorption indicators were recorded at 50-75% higher after a 4-6 month space flight than pre-flight (Smith, et al., 2005).

Though remaining largely dormant, osteocytes are thought to control the process of osteogenesis via stimulation of osteoblastic and osteoclastic activity within a basic multicellular unit (BMU) (Taylor, et al., 2007). A single BMU

consists of active multinucleated osteoclasts that resorb the bone matrix at the front of the BMU, active osteoblasts at the rear of

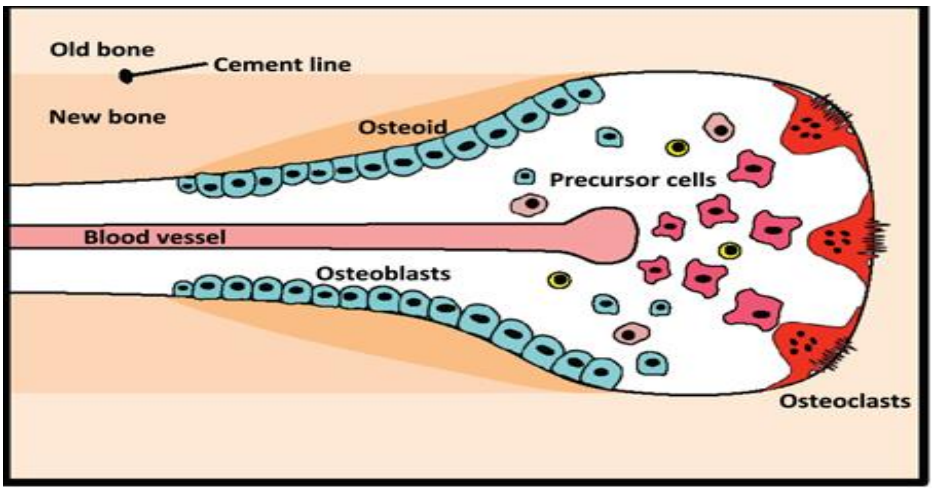

Figure 3. Schematic diagram of a basic multicellular unit (BMU) (Sims & Martin, 2014)

the BMU that form osteoid, which is later mineralised forming new bone matrix (Figure 3) (Buenzli, Jeon, Pivonka, Smith, & Cummings, 2012). The cell distribution within a BMU moves in wave-like formations, changing cell densities corresponding to the differentiation and apoptosis rates (Buenzli, Pivonka, & Smith, 2011). Noble, et al. (2003) established a biphasic response to mechanical load, forming a U-shaped relationship between mechanical strain an osteocyte survival. Made possible by the ability of both living and dying osteocytes to recruit osteoclasts to remodeling sites (Kogianni, Mann, & Noble, 2008). During periods of local strain where microstructural damage can be high, damage repair by BMUs is more efficient, being guided towards the local strain (Martínez-Reina, Reina, Domínguez, & García-Aznar, 2014). Conversely, disuse/under-loading promotes osteocyte apoptosis within the BMU (Bakker,

Klein-Nulend, & Burger, 2004) (Basso & Heersche, 2006) and recruitment of osteoclasts (Aguirre, et al., 2006). Apoptotic osteocytes have been shown to release RANKL expressing apoptotic bodies involved in recruiting osteoclasts, reliant on the tumour necrosis factor-α of osteoclast precursors (Zhang, Heulsmann, Tondravi, Mukherjee, & Abu-Amer, 2001). This strong relationship between RANKL and TNF-α indicates a positive feedback loop by which inflammatory bone osteolysis (as seen in osteoporotic patients) leads to the hastening of RANKL induced osteoclastogenesis and therefore further osteolysis (Schett & Teitelbaum, 2009). Osteocyte cell death can sharply rise in concurrence with several pathological conditions such as osteoporosis (Plotkin, et al., 1999) or osteoarthritis (Findlay, 2007) preceding an increase to skeletal fragility. This increase in skeletal fragility is thought to be caused by two different aspects of microdamage; a positive feedback loop created by simultaneous bone loss and microdamage (Burr, et al., 1997), and the decreased ability to sense microdamage and signal the necessity of repair to other bones (Verborgt, Gibson, & Schaffler, 2000). Carter, et al. (2013) found that the fragility of mature bone is due to subsequent reduction in cell capability and not cell apoptosis, specifically a decrease in lacunar density, consequently the osteocyte count was less significant compared to the lacunar networks overall loss of volume. Britz, et al (2012) observed a significant reduction in osteocyte lacunar

density and volume when the tibial diaphysis of a rat was subjected to under-loading through disuse and immobilisation. In addition, hypermineralization of osteocyte lacunae has been shown to occur in patients who suffer from osteoporosis (Carpentier, et al., 2012), changing aspects of bone fluid flow across the osteocyte lacunocanalicular network, in turn affecting

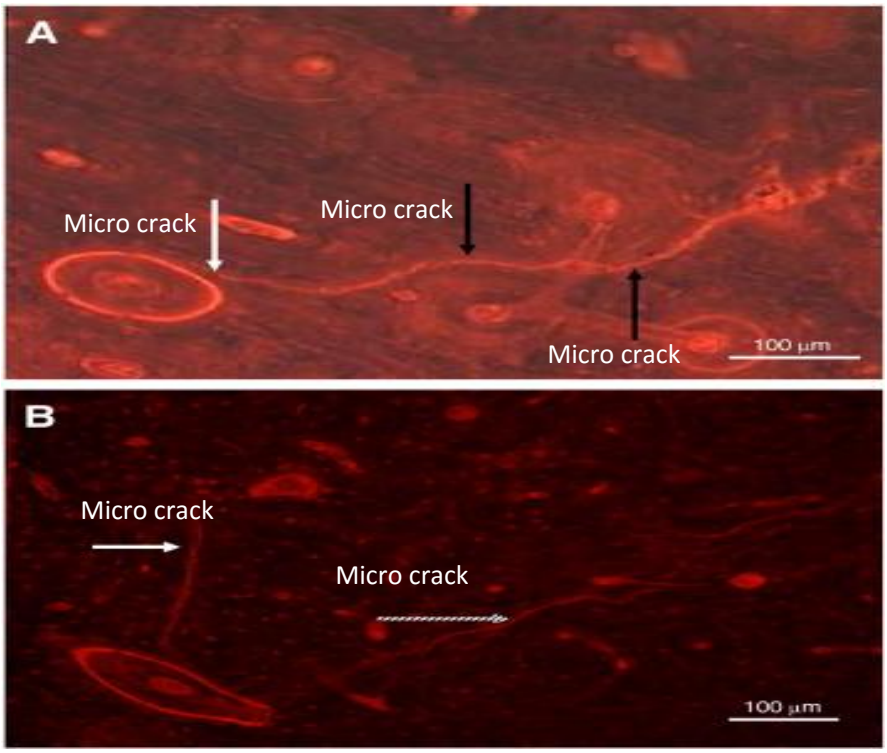

Figure 4. An example of microcracking in cortical bone, viewed using green epifluorescence (Kennedy, et al., 2008).

osteocyte function and viability (Bonewald, 2011). Similarly Vashishth, et al (2000) showed an exponential increase in porosity and microcrack density (Figure 4) paired with a decline in osteocyte lacunar density demonstrating a minimum population of osteocytes is required for a functioning network. Moreover, interstitial bone has been found to express a variance

in osteocyte lacunae neighbouring regions of microdamage when compared to areas isolated from microdamage (specifically a 16% reduction). In bone with an osteocyte lacunar density below the lower boundary of a typical subject, increased likelihood of microdamage was observed at a rate of up to 3.8 times higher. Typical osteonal bone was shown to have 30% of its average lacunar density to be below the lower boundary, when adjacent to microcracks this Figure rises sharply reaching up to 83% (Qiu, Rao, Fyhrie, Palnitkar, & Parfitt, 2005). This reduction in osteocyte lacunar density can also be ascribed to a difference in extremely localized variation in loading conditions causing morphological differences (elongation and flattening) to the lacunae specifically in the lateral and medial regions of the femur (Carter, et al., Variation in osteocyte lacunar morphology and density in the human femur — a synchrotron radiation micro-CT study, 2013). Additional morphological changes have been observed in the human rib, as osteocyte lacunar density increases Haversian canal area decrease, contracting up to 4-5% of it's the osteon area before bone apposition ceases (Qiu, Fyhrie, Palnitkar, & Rao, 2003). Indicating a possible link between mechanical loading (under-loading), osteocyte lacunar density and Haversian canal size.

1.1.3: Bone Signalling Molecules

Mechanical under-loading through disuse is associated with changes in several signalling molecules, Gerbaix, et al. (2015) observed a direct correlation between bone loss, inhibition of periostin and subsequent increase of sclerostin in hindlimb suspended mice. Furthering this periostin has been shown to have an effect on the ability of PTH to improve cortical structure and strength, impairing PTH in its absence (Bonnet, Conway, & Ferrari, 2012). Additional studies have found similar benefits of PTH on bone mass and strength, Neer, et al. (2001) found significant increases in bone mineral density of the spine (between 9 and 13 % increase compared with the placebo) and femoral neck (3 and 6% increase compared with the placebo) of post-menopausal, osteoporotic women, dependant on the dose, indicating a relationship between bone formation and PTH activity. Similarly, PTH signalling during exercise was shown to mediate the load response within the cortical bone (Gardinier, Al-Omaishi, Morris, & Kohn, 2016). Collagenase-3, an extracellular membrane degrading enzyme (Ohuchi, et al., 1997) displays heightened expression by PTH activated osteoblasts resulting in a subsequent increase bone resorption (Kusano, et al., 1997). However the production of insulin-like growth factor-I (IGF-I) stimulated by PTH stimulates osteoblast proliferation resulting in a higher rate of bone formation (Linkhart & Mohan, 1989). RANKL is a membrane protein produced by osteoblasts, which when expressed

induces osteoclast maturation and bone resorption (Rana, Schultz, Freeman, & Biswas, 2012). Its receptor activator NF-κB (RANK) lies on the surface of haematopoietic cells. Initiating microdamage by mechanically scraping osteocyte surfaces prompting local secretion of RANKL inducing the activation of the initial phase of osteoclastic cell formation,therefore, encouraging the formation of new bone in acutely specific regions (Kurata, Heino, Higaki, & Väänänen, 2006). Similarly exposed to PTH, RANKL secretion is stimulated leading towards an increase in osteoclastogenesis and consequently a reduction in bone mass (Coetzee, Haag, & Kruger, 2007). When induced by PTH, osteocytes, not mature osteoblasts have been found to be the major source of RANKL. In the same study, a 70% reduction in cancellous osteoclast count occurred when RANKL was deleted from osteocytes and osteoblasts without the distant transcriptional enhancer identified as the distal control region (DCR) used to mediate PTH and RANKL expression (Xiong, et al., 2014). Stimulation of osteogenesis by RANKL is controlled by the ratio of OPG to RANKL as OPG stops the binding of the RANKL ligand to the RANK molecule as can be seen in Figure 5.

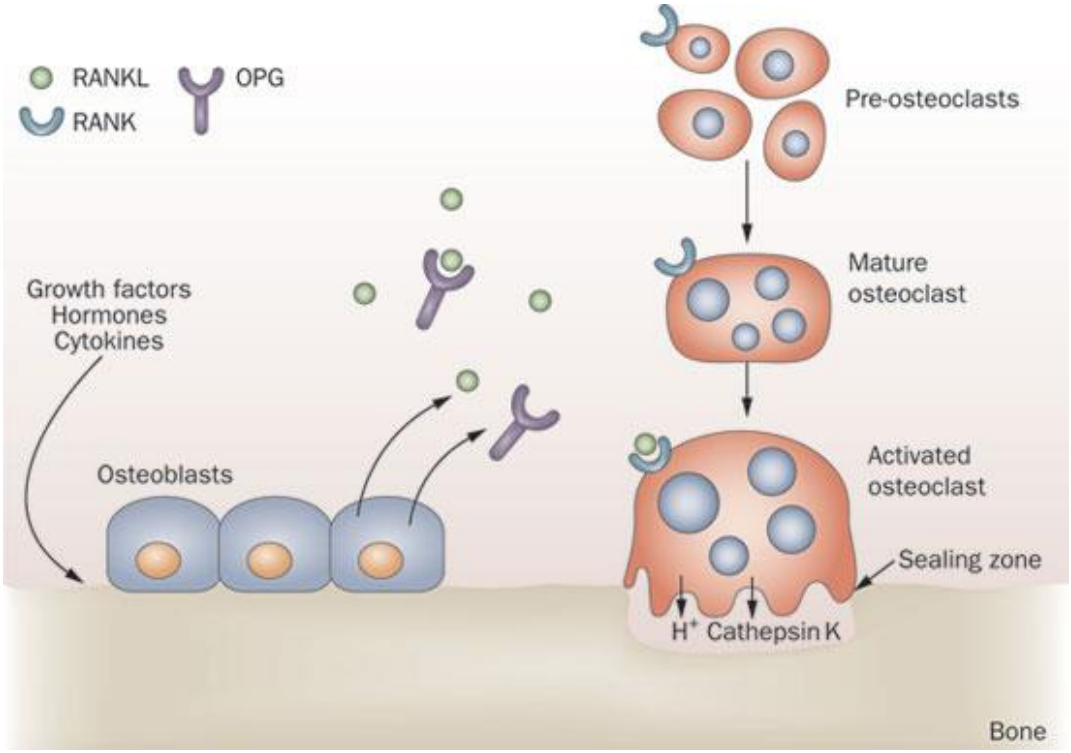

Figure 5. Model illustrating the mechanisms by which OPG and RANKL regulate bone resorption and bone formation through osteoblast/osteoclast interaction.

(Lewiecki, 2011)

When applied to a model of mechanical loading OPG/RANKL ratios have been shown to correlate (Tyrovola & Odont, 2015) with that of Frosts (1987) "mechanostat theory", indicating that OPG and RANKL are key moderators of bone loss in an underloaded model.

In postmenopausal women, the RANKL/OPG ratio is a useful marker for predicting the onset of osteoporosis, having an inverse relationship with bone mass density (Jabbar, et al., 2011). Treatment of OPG in tail-suspended mice, reduced femoral endocortical resorption by 24% compared to placebo-treated groups, microhardness also increased by 5.7% compared to placebo-treated tail-suspended mice, returning it to nonsuspended control

levels (Bateman, et al., 2000). Another key signalling molecule, interleukin (IL)-1β encourages osteoclastogenesis by stimulating the production of OPG ligand (OPGL), promoting bone resorption and therefore bone loss (Hofbauer, et al., 1999). Moreover, in patients suffering from rheumatoid arthritis, IL-1β was shown to encourage up-regulation of osteoblastic apoptosis (Tsuboi, et al., 1999)indicating a possible link between IL-1β expression and the reduction in osteoblast cellular integrity seen in skeletal unloading (Nabavi, Khandani, Camirand, & Harrison, 2011). Kulkarni et al, (2012) found osteoclastogenesis was inhibited regardless of the concentration of IL-1β when the bone is subjected to mechanical loading. Additionally, inhibition of the clustering of osteoclast precursors (a key component of bone formation) was observed when exposed to mechanically loaded IL-1β-treated osteocytes.

1.2.0: Pathologies Associated with the Skeletal Loading Regime

1.2.1: Osteoporosis

Osteoporosis is a disease of bone characterised by an inadequate amount and/or faulty structure of bone subsequently leading to reduced bone strength and fragility. Predisposition to bone fracture is therefore heightened (Kanis, Melton III, Christiansen, Johnston, & Khaltaev, 1994).Originally coined in the 19th Century, the term osteoporosis (meaning 'porous bone') was initially a histological diagnosis, since then, however, it has developed to mean 'bone that is mineralised normally but is of reduced quantity' (Figure 6) being measured by a reduced bone mineral density (BMD) through radiological analysis (Arden, 2006).

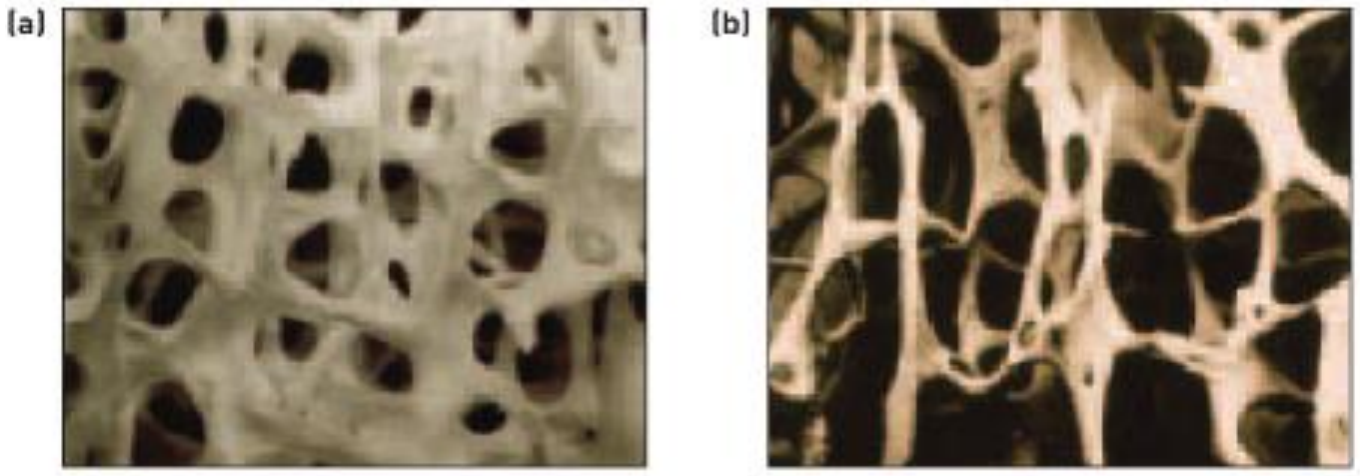

Figure 6: (a) Cancellous bone (b) Osteoporotic Bone. Reproduced from (Litwic & Dennison, 2014)

Further diagnosis includes previous fractures (World Health Organization, 2004). The onset of osteoporosis is not fully understood however it is thought to be triggered by disproportionate resorption and an insufficient response to the increased resorption during bone remodeling (Vigorita, 1999). Over 500,000 people receive hospital treatment for fragility fractures every year as a result of osteoporosis (NHS, 2016). Osteoporotic fractures are more frequently observed in older patients, with the largest incidence rate in elderly, post-menopausal women with fracture rates as high as 40% in white women over 50 comparable to the 13% fracture rate seen in white men of the same age (Melton, Chrischilles, Cooper, Lane, & Riggs, 1992). As we see a larger, increasing aging population (average lifespan is predicted to raise by another 10 years by 2050 (Centers for Disease Control and Prevention, 2003)) a simultaneous rise in prevalence of age-related diseases also occurs, for example in the USA a large probability sample survey found 20% of white postmenopausal women suffered from osteoporosis of the femoral neck with a similar statistic (20%) for men above 50 suffering from osteoporosis in general (Melton J. L., 2001). In the UK the statistic is slightly higher with nearly 25% of women over 50 afflicted with osteoporosis (Kenny, 2014). As aging occurs so does bone growth, showing a particularly severe change in density, reaching peak density early in life at around the mid to late 20's (O'Flaherty, 2000). After this, peak BMD naturally declines. On average a severe drop in BMD is seen at the age of 50, predominantly in women correlating with the post/menopausal period (53.2% among women and 20.7% among men)

(van Staa, Dennison, Leufkens, & Cooper, 2001). The causal link between rapid bone loss and menopause can be mainly attributed to a reduction in oestrogen levels. Therefore oestrogen therapy has been used as a successful treatment for patients suffering from menopausal related bone loss (Lindsay, et al., 1978) (Schneider, Barrett-Connor, & Morton, 1997) (Munk-Jensen, Nielsen, Obel, & Eriksen, 1988). Additionally, women with a lower BMD before the start of menopause have been shown to have a greater rate of bone loss, therefore are at a greater risk of fracture (Riis, Hansen, Jensen, Overgaard, & Christiansen, 1996).

Several secondary factors such as marrow-related disorders, eating disorders, disorders of the gastrointestinal or biliary tract, endocrine disorders, and adverse effects of drug therapy, renal disease, cancer, and immobilization can influence the onset of osteoporosis (Fitzpatrick, 2002). Patients who are at a higher risk of osteoporosis would see a greater amount of bone loss through any reduction in mechanical load Tannenbaum, et al. (2002) found 32% of postmenopausal women in their study (55 of 173 women) presented secondary causes of bone loss. In men, secondary disorders or causes are found to be the most prevalent source of osteoporosis (Korpi-Steiner, Milhorn, & Hammett-Stabler, 2014), especially the prescription of glucocorticoids (Adler, 2013). Prescribed to treat conditions such as rheumatoid arthritis or chronic obstructive pulmonary disease (Canalis, Mazziotti, Giustina, & Bilezikian, 2007), glucocorticoid-induced osteoporosis happens in two phases; a rapid decrease in BMD caused by an increase in bone resorption, up to a 27%

reduction in total bone volume in the first 12 months of glucocorticoid treatment (LoCascio, et al., 1990) resulting in up to 75% higher risk of fracture (Van Staa, Leufkens, Abenhaim, Zhang, & Cooper, 2000) followed by a slower decline in BMD thought to be the result of impaired bone formation (O'Brien, et al., 2003). Conversely, plasma glucocorticoid levels show no correlation with BMD in underloaded models (Halloran, Bikle, Cone, & Morey-Holton, 1988). However, Braith, et al (2003) found mechanical loading through exercise in patients who suffered from glucocorticoid bone loss after heart transplant surgery increased BMD whereas BMD was significantly reduced in the control group. Showing a correlation explained by Wolff's Law (Frost H. M., 2004).

1.2.3: Skeletal Models – Effects of Loading and Under-loading

Wolff's law is the rule which describes the adaptive change loading has on the bones of an individual if loading increases then the bone will begin the process of remodeling (Barak, Lieberman, & Hublin, 2011), strengthening to resist the load placed on it. Figure 7 clearly highlights this relationship between

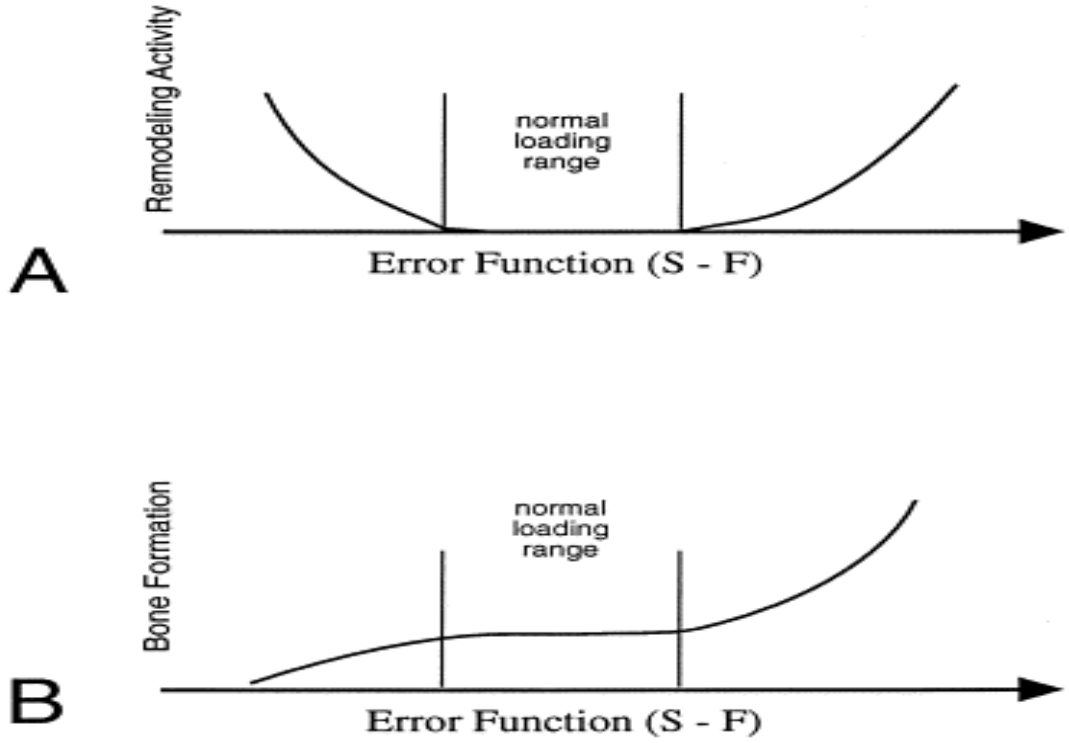

Figure 7: The relationship between mechanical loading, remodeling activity, and bone formation. Where error function is daily load – normal loading pattern

(Turner, 1998)

loading and remodeling. If exposed to a reduced load then Wolff's law takes the form of a reduction in BMD as seen in diseases such as disuse Osteoporosis (osteoporosis as a result of under-loading

bone) which can be derived from two sources; a failure of bone to attain optimal BMD and strength, if during the build-up of bone mass, disuse had occurred and an accelerated rate of resorption versus a slower rate of formation (Raisz, Bilezikian, & Martin, 2008). Several studies have observed a causal link between under-loading and osteoporosis (bone loss) in a wide variety of different models, for example, Vico, Novikov, Very, & Alexandre (1991) established a difference in bone loss seen in tail-suspended rats when compared with that of rats experiencing weightlessness during spaceflight. Both models experienced bone loss however trabecular bone loss was more widespread in spaceflight rats, conversely, the rate of bone resorption was unchanged in spaceflight rats but tail-suspended rats showed a twofold increase. Furthering this, tail-suspended rats exhibit a decrease in bone formation, however after 12 days bone formation had returned to normal, suggesting under-loading only has a temporary effect on bone formation (Globus, Bikle, & Morey-Holton, 1986). A related study looking at the effect of loading on bone formation discovered an increase in BMD of the lumbar vertebrae in the hind-limb suspended mice (Figure 8) (Zhao, Dodge, Ledet, & Yokota, 2011). Moreover, similar studies correlate with previous findings, namely that hindlimb/ tail-suspension in rats and mice demonstrate increases in bone resorption whilst bone formation was inhibited (Wronski & Morey, 1982) (Matsumoto, et al., 1998) (Ishijima, et al., 2001). Another animal model by which

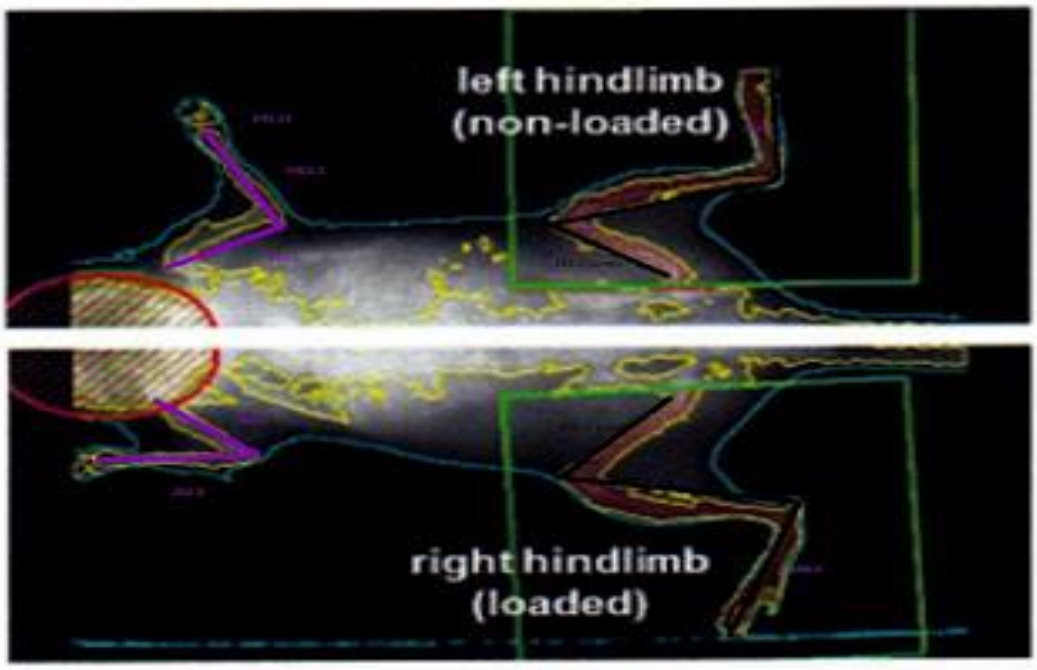

Figure 8: PIXImus measurements of mice hind limbs (Zhao, Dodge, Ledet, & Yokota, 2011)

immobilization has been studied is that of the dog, Grynpas et al, (1995) observed a significant decrease in cortical bone density within the immobilized control group of 6 beagle dogs. The decrease in bone density was attributed to significant hypomineralization of the trabecular bone. A previous study observed the effect an AO plate fixator placed on the right femur of dogs would have on the bone in an attempt to induce bone loss. They detected a significant difference in bone mineral mass per centimetre length of the AO-plated femora caused by the acute resorption often seen in bone disuse studies (Tonino, Davidson, Klopper, & Linclau, 1973). Likewise, Thomas, et al., (1996), used plate fixators to simulate immobilization from the tibia to the metatarsus of adult female sheep. After 12 weeks a 29% decrease

in trabecular bone volume was observed. Furthering this Loveridge, et al., (2011) used external fixator bars on left calcaneus of ewes, reducing maximum local loads by 50%. This reduction in maximum load saw a decline in cortical area and thickness after 16 weeks with an increase in mean canal area of $62.5 \pm 15 \mu m^2$. In one study, sheep that were subjected to immobilization over a period of 12 weeks found no significant difference between the bone mass content (BMC) of subjects that had fixator bars removed for 20 minutes a day allowing for free movement and weight bearing on the left calcaneus, when compared to subjects that did not have their fixators removed (21% and 22% reduction in BMC respectively) (Skerry & Lanyon, 1995). This suggests that it is prolonged exposure to a reduced load that causes a reduced bone mass and not simply brief changes in loading environment. Research on the ovine calcaneus can be derived from it's similar morphology with that of the human femoral neck , producing comparable results when looking at fragility fractures (Loveridge, et al., 2011). These results can only be compared because of the similarities between the principal loading axis of both models (Figure 9). In cases of loading, significant increases in the thickness of cortical bone along the inferior weight-bearing region of the human femoral neck have been observed (Narra, Viik, Hyttinen, & Sievänen, 2013).

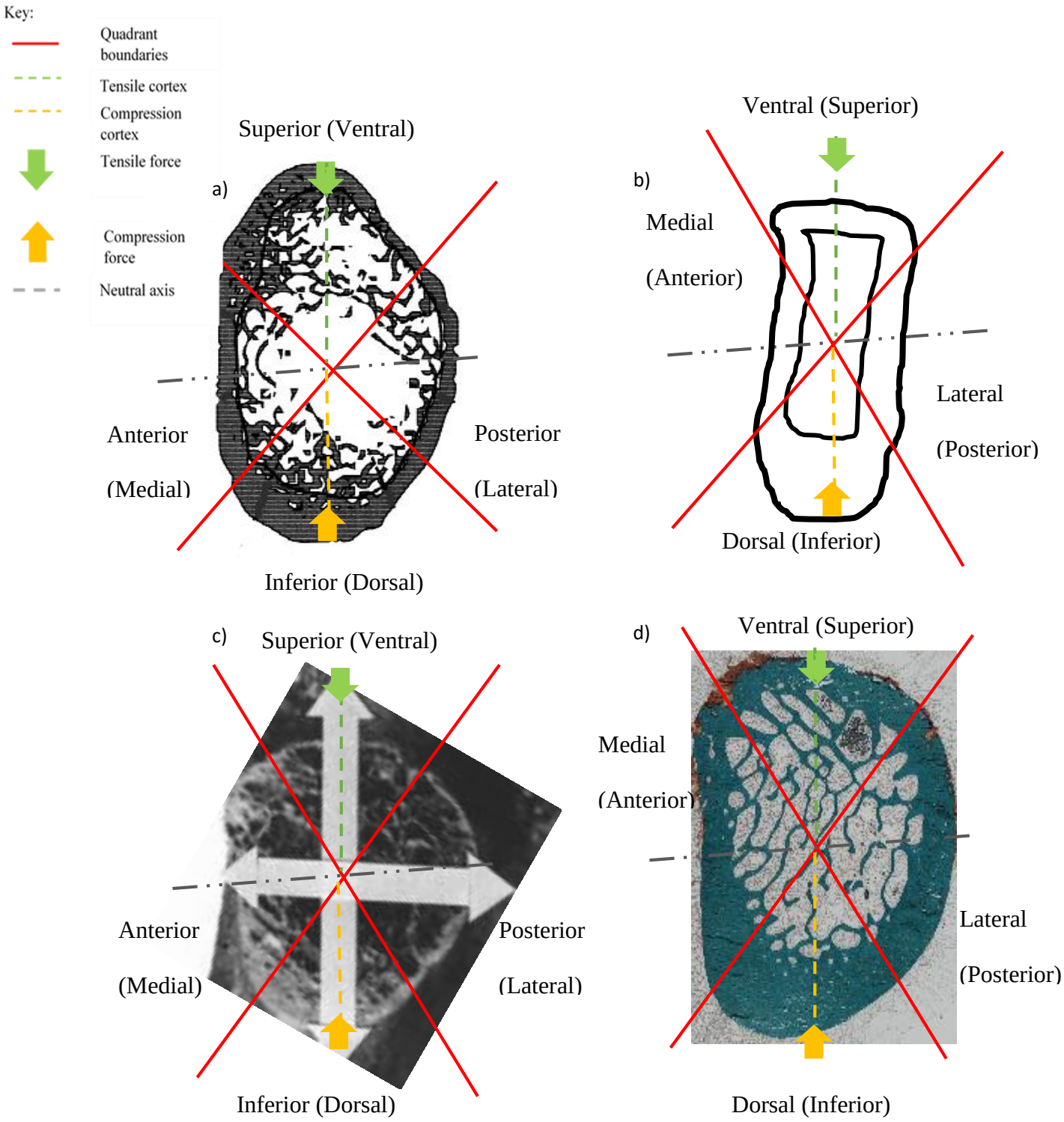

Figure 9. a) Schematic cross section of the femoral neck. Adapted from (Bell, et al.). b) An illustration of a cross section of the ovine calcaneus. c) Image capture of the frontal femoral neck. Modified from (Antonelli, 2001). d) High-Resolution image of the ovine calcaneus, image provided by Dr Jon power.

All Images have labelled quadrants with their representative section within the other model shown in brackets e.g. The "dorsal" quadrant of the ovine calcaneus is structurally similar to the "(inferior)" section of the human femoral neck etc.

Similar results have been observed in the ovine calcaneus where increased osteonal remodeling was found to be closely linked to a greater loading strain in the cranial (superior) axis (Lanyon, Magee, & Baggott, 1979). The cortical width of the femoral neck is considerably lower when subjected to periods of under-loading in humans (Mayhew, et al., 2005) likewise cortical width of the sheep calcaneus is also reduced (Loveridge, et al., 2011). An increase in osteoid to bone surface ratio has also been observed in the femoral neck (Power, et al., 2003) indicating a remodeling imbalance leading to a reduction in bone mass. Previously Thomas, et al., (1995) found the same relationship between under-loading and osteoid increase, almost doubling the percentage covering of osteoid on the bone surface from 3.9% in the control to 7.7% in the immobilized calcaneus. BMD shows similar patterns in the human femoral neck (Magnusson, Lindén, Karlsson, Obrant, & Karlsson, 2001) (Leblanc, Schneider, Evans, Engelbretson, & Krebs, 1990) (Fox, et al., 2000) and ovine calcaneus (Skerry & Lanyon, 1995) (Thomas, et al., 1996) namely that it is reduced in an underloaded model.

Loveridge, et al., (2011) observed a marked decrease in %cortical area (diff; - 10.6%) and cortical thickness (diff -0.13mm) in the under-loaded calcaneus at 16 weeks. In addition mean canal area was increased (diff +62.5±15μm^2). These findings suggest a direct relationship between underloading of the ovine calcaneus and

increased bone loss within the ovine model. However further study into this relationship can be achieved through the use of greater specificity; namely rather than measuring the whole calcaneus (Loveridge, et al., 2011) done by simply generating data for the each of the four quadrants(as can be seen in figure 9). This would in turn provide a greater understanding as to the exact area and along which loading axis bone loss of the ovine calcaneus can be seen.

1.2.4: The Aims and Objectives

It is well documented that the skeleton responds to reduced mechanical load by a reduction in bone mass. While the relationship of diminished bone mass with decreased mechanical load is well established (Frost H. M., Skeletal structural adaptations to mechanical usage (SATMU): 2. Redefining Wolff's Law: The remodeling problem, 1990), the rates by which a structural change and/or bone turnover rates occur are less clear. This study addresses these issues via histomorphometric measurements of structural parameters specifically cortical porosity, cortical width and bone remodeling (bone formation). Changes in these parameters were to consider possible mechanisms leading to a reduction in bone strength in response to a reduction in mechanical load.

The purpose of this study was to verify a link between bone loss and mechanical under-loading within the temporal model of the ovine calcaneus.

Chapter 2.0: Materials and Methods

This histological study was based on an ovine model of under-loading where all previous surgical and histological procedures were already completed. The histological procedures were carried out at the University of Cambridge by Dr. J. Power and under the funding of BBSRC research grant BB/D004624/1 (Dr. Nigel Loveridge principle investigator) (Loveridge, et al., 2011).A brief overview of the process from bone acquisition to analysis is demonstrated in figure 10:

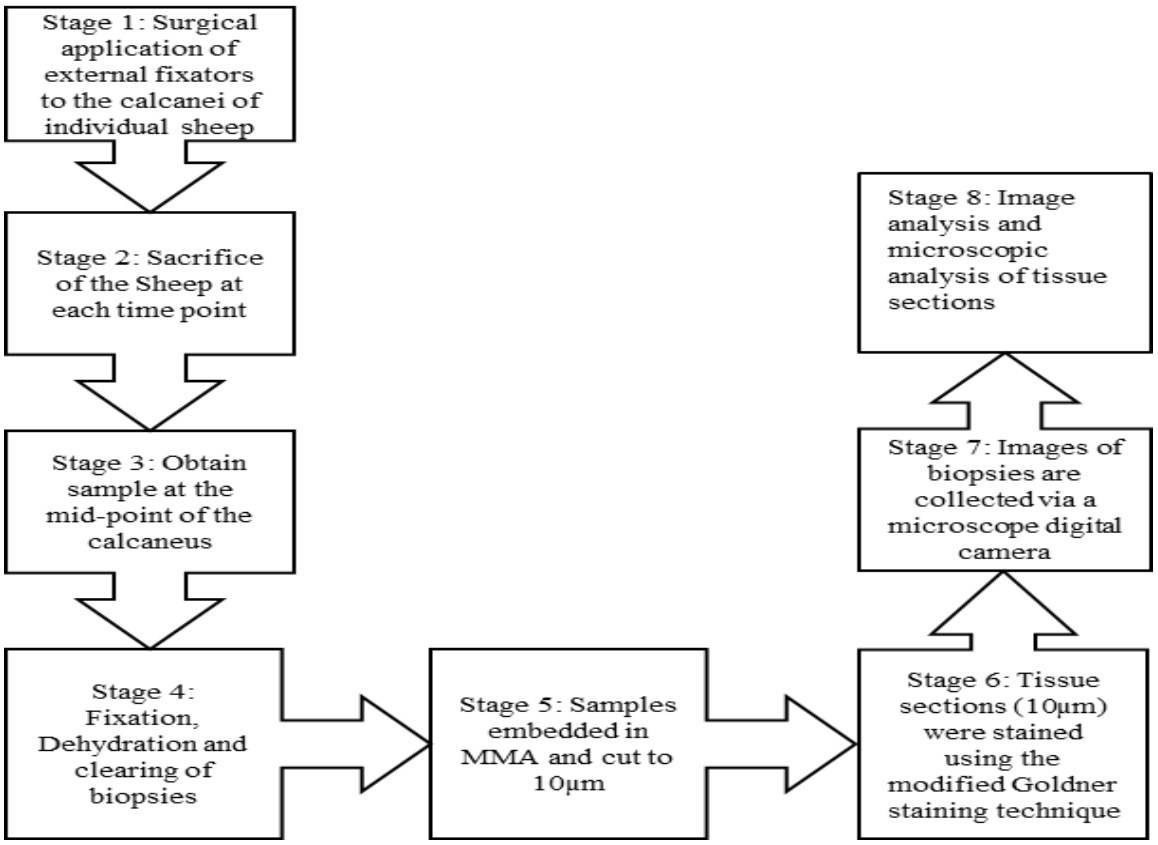

Figure 10: Generalised flow chart of the methods

The surgical procedure undertaken above in order to produce a state of under-loading is briefly described in the following section.

2.1.1: External Fixation of the Ovine Calcaneus

A fixator bar (Figure 11 (b)) was surgically applied around the calcaneus of 12 age-matched ewes , immobilising the tarsal region

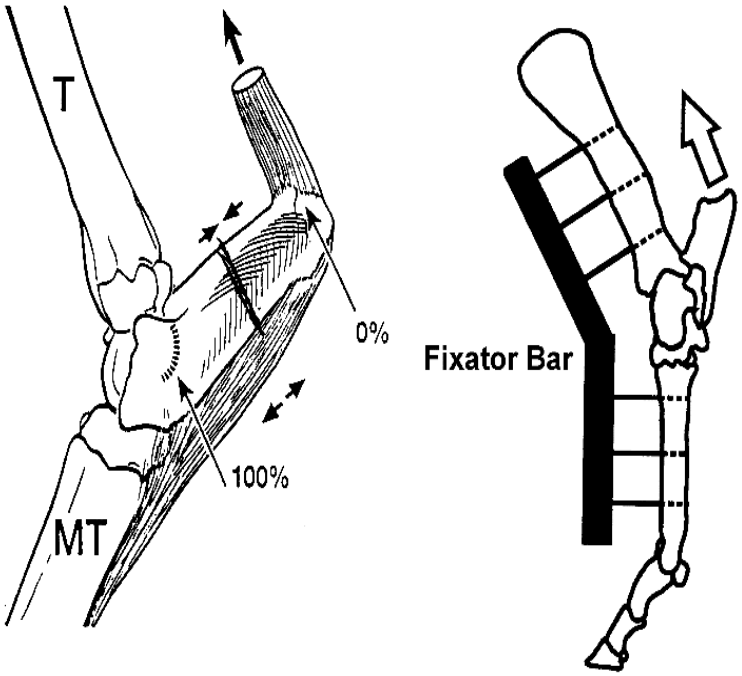

Figure 11: (a) The ovine calcaneus highlighting the mid-point at which the bone was cut (b) Placement and appropriate force reduction of the fixator bar (Loveridge, 2004)

of the sheep. This procedure caused a 50% reduction in principal strain magnitudes on the calcaneal cortices (Loveridge, et al., 2011). Immediately after fixation 6 animals were sacrificed, this group served as the time 0 group (control (animals experiencing a normal mechanical loading regime)). At week 4 another 6 animals were sacrificed and a final group at 16 weeks (representing the underloaded groups). Following sacrifice, the calcaneus was removed by manual extraction and the cross-section of the calcaneus cut from the midpoint of the bone as can be seen in Figure

11 (a). The calcaneus then was processed for histology where sections were taken from the midpoint using the following method.

2.1.2: Histology

Cross-sections of the ovine calcaneus were obtained from the mid-shaft of each sample. They were then fixed in 10% buffered neutral formalin for 10 days at 4°C and washed in distilled water for 30 minutes before dehydration. A series of ethanol dilutions were used for dehydration, the dilutions were as follows; 30, 50, 70, 90 and 2x changes in 100% ethanol with 24hrs between each change. Following dehydration, the biopsies were cleared in xylene with two changes (24hrs between each change). After clearing, samples were embedded in methyl methacrylate (MMA) by the method of Zanelli Joan, et al., (1993). Sections were cut (25 µm and 30 µm, measured by a micrometer) on a polycut E-sledge microtome (Leica, Milton Keynes, UK) and were stained using the modified Goldner staining technique. Each bone sample provided one section for analysis.

2.2.1: Microscopic analysis of histomorphometric parameters relating to under-loading of the ovine calcaneus

Eighteen microscopic cross sections of the calcaneus were mounted onto microscope slides and images were gathered at x5 objective magnification using Objective Imaging® software (Cambridge, UK). This process was carried out at Cambridge University by Dr. J. Power. Cross-sections of the calcaneus were selected for microscopic analysis, with 6 at day 0 (control), 5 at 4weeks and 6 at the final time point of 16 weeks post application of under-loading. Only 5 cross-sections were examined at week 4 because one of the digital images for that time point was corrupted therefore making computer analysis not possible. Structural parameters (cortical width and porosity) were analysed using ImageJ software (ImageJ, https://imagej.nih.gov/ij/).

Each cross-sectional bone image was analysed in four separate regions which experience similar anatomical and loading regimes to their corresponding regions in the human femoral neck. Medial which is structurally similar to the anterior region of the human femoral neck, Dorsal corresponding to the inferior region of the femoral neck, Lateral the posterior and Ventral the superior region (Figure 12).

(a)

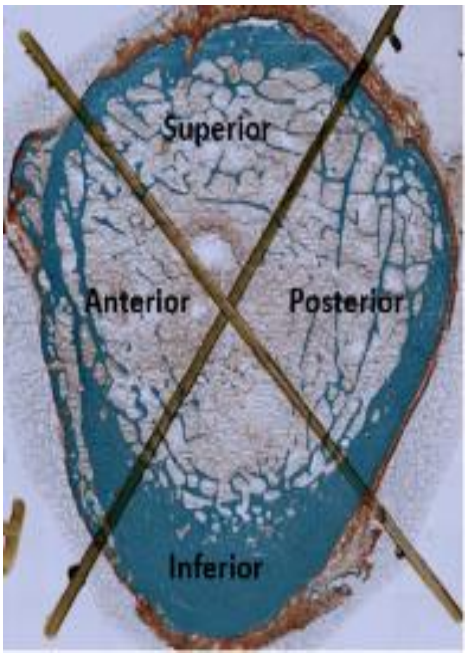

(b)

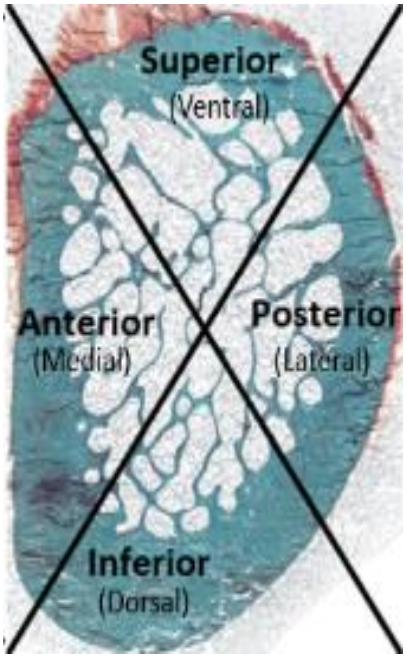

Figure 12: (a) Human femoral neck cross section displaying the four quadrants (image courtesy of Dr. Jon Power) (b) Ovine calcaneus cross section showing the four quadrants, ovine model quadrant labels are bracketed (images courtesy of Dr. Jon Power)

2.2.3: Cortical Width Analysis

The measuring of the cortical width of a bone image was achieved firstly by splitting the image into quadrants for analysis. A quadrant was measured by a line running from opposite corners through the centre point. Each quadrant was then further split into 20 sections each equal in size, providing 18 data points (not including points of data from each corner and midpoint). From here lines were drawn from each of the 18 data points on the extremity of the image into the centre point (Figure 13). The cortical width

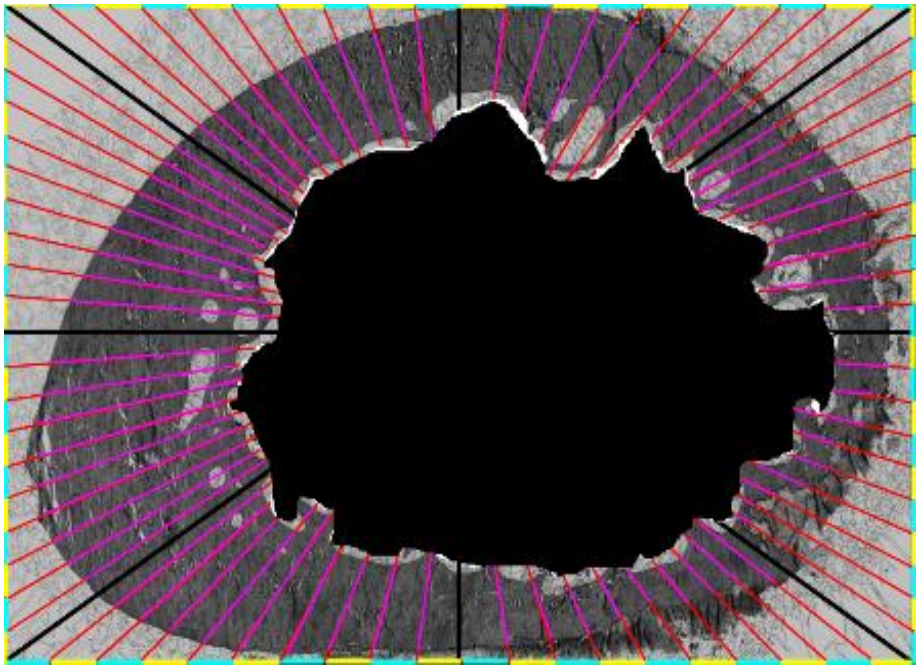

Figure 13: Measuring the width of the ovine calcaneus.

was determined by measuring the distance in mm from the boundary of the endocortical surface to the periosteal edge. Where cortical canals intercepted the endosteal/periosteal measurement (cortical width) this distance was subtracted from the value. The endosteal surface was defined prior to measurement by the method of Brown et al (1987). Width was measured in mm using a scale factor of 537.02 pixels/mm. Figure 14 illustrates this method pictorially.

2.2.4: Determination of Total Cortical Porosity

Cortical porosity was quantified using ImageJ software firstly by creating a red/blue/green (RBG) stack of the image and subtracting the red and blue stacked images. This provided a grey scale image allowing for a clearer distinction between canals and potential artifactual sectioning damage within the tissue. Following this, the circumference of each canal area was traced and filled (Figure 14(a). The image was then thresholded as to create a binary image that allowed for discrimination between the filled in canals and the rest of the bone (Figure 14(b)). Finally, a measurement of the area of each pore was gathered using the "analyse particles" command in ImageJ. After this has been achieved, the same method was used on the original image except for the total bone (Figure 14 (c)) and the marrow cavity area (Figure 14 (d)) which were filled independently allowing for a separate measurement of each feature. Applying the calculation of total bone – total marrow cavity to

determine the cortical area, this was then used in a separate equation:

$$\left(\frac{total\ porosity\ area}{cortical\ area}\right) \text{x}100$$

providing the total % porosity of the cortical bone. This method was repeated in each respective quadrant allowing further analysis of % porosity by comparison between segments.

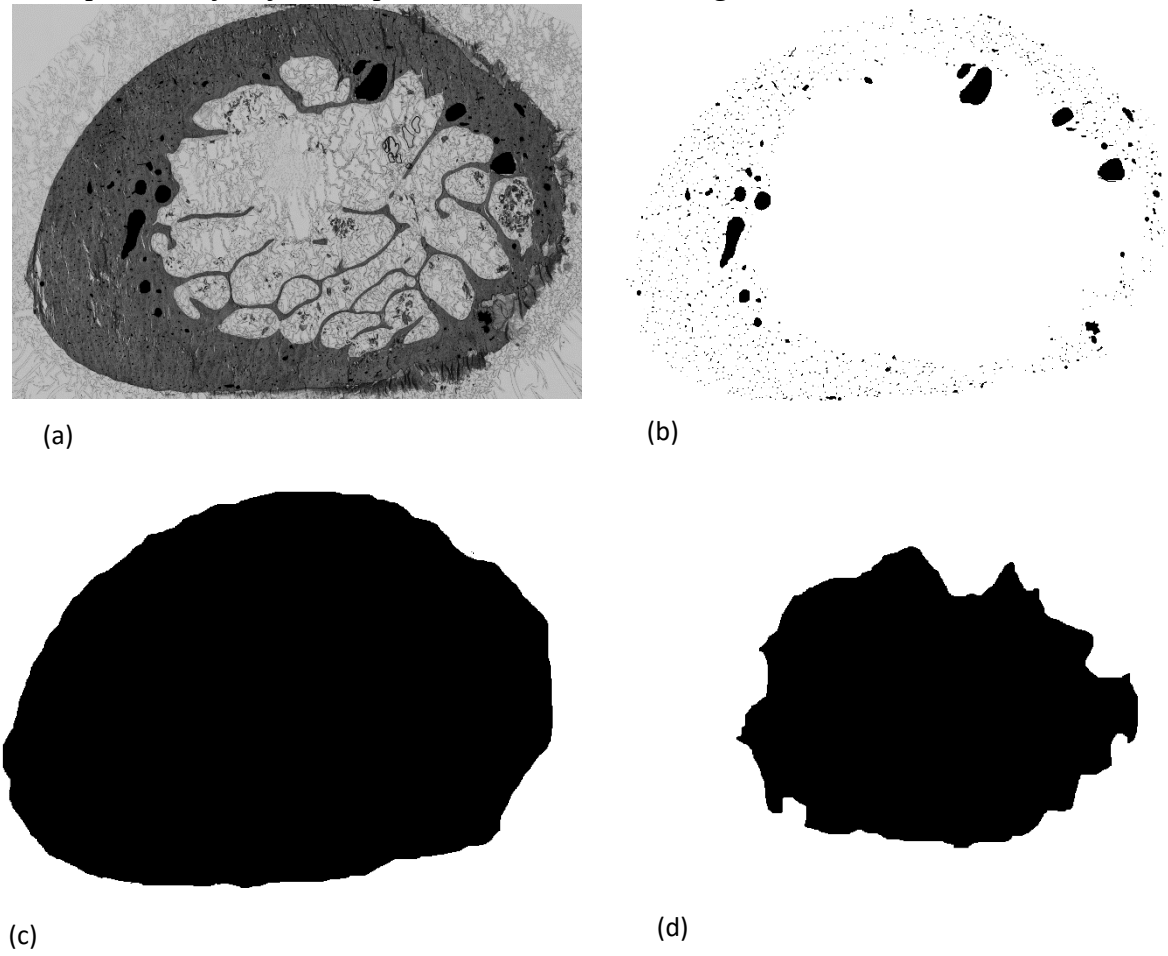

Figure 14: (a) An example of the ovine calcaneus with all canals filled. (b) An ovine calcaneus after the canals have been filled and the image threshold. (c) The complete calcaneus filled. (d) The filled marrow cavity of the calcaneus after being threshold.

2.2.5: Determination of cortical bone remodeling - % of canals undergoing bone formation

Quantifying cortical remodeling was achieved manually through the use of microscopy on previously acquired bone sections, mounted on microscope slides and stained using modified Goldners trichrome method. A Nikon E2000 microscope (at x20 obj. mag.) and a mechanical hand tally counter were used to track the total number of canals demonstrating the presence of osteoid (Figure 15). This test was performed blind and repeated nine times for each individual slide. In order to generate a regional analysis (medial, lateral, dorsal and ventral) each slide was split into four regional quadrants using a thin point permanent marker pen. The proportion of the percentage of forming canals (as an index of bone remodeling activity) was calculated as:

$$\left(\frac{no.\ of\ forming\ canals}{total\ canal\ number}\right)\ \text{x}100$$

This was performed at the level of the whole section and for each individual anatomical region.

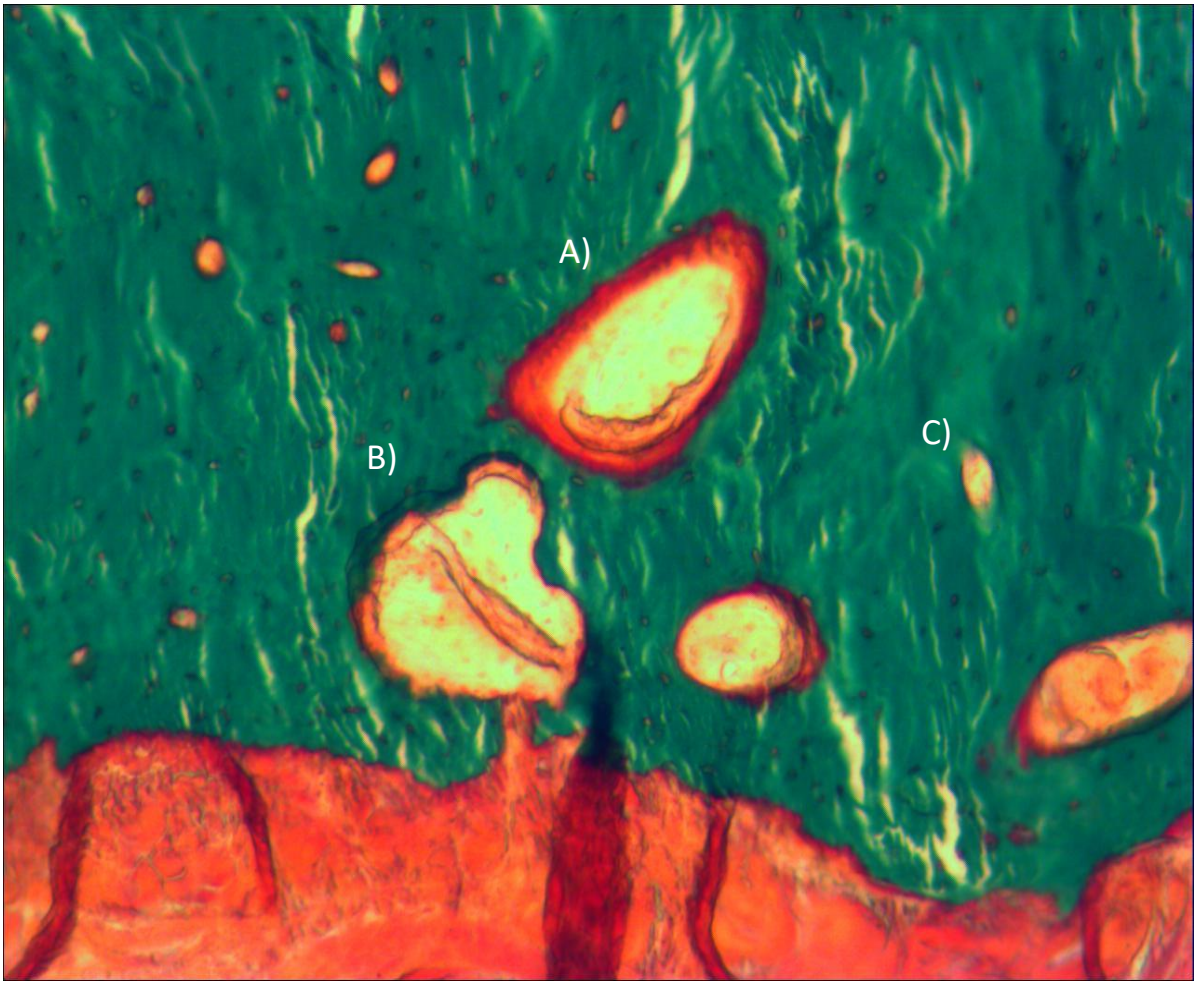

Figure 15: Goldner's Trichrome stained cortical bone (x20 obj image) demonstrating Haversian canals undergoing bone remodeling. A) Forming canal indicated by a layer of newly synthesised, non-mineralised bone (termed osteoid). B) Resorbing canal, demonstrating a crenelated (irregular or pitted) surface denoting resorptive cavities. C) Quiescent canal identified by a smooth surface. (Image provided courtesy of Dr. J. Power)

2.3.1: Statistical Analysis

All statistical analysis was performed using IBM Statistics SPSS 20. All sectional data was first tested for a normal distribution ($p>0.05$) through the use of a Shapiro-Wilk test, if the data was normally distributed then a one-way ANOVA parametric test was used to assess the variability between means, significant data was then further analysed with a post hoc Dunnett test. Data was determined as significant when $p<0.05$. Non-normally distributed data was subject to the non-parametric Kruskal-Wallis test if that data was significant ($p<0.05$) then a Mann-Whitney U test was performed as to distinguish the significance between the results at each time point e.g. between day0 and week 16, week4 and week 16, day0 and week4. Where data was normally distributed the means ± standard error (SE) were calculated for each region. Non-normally distributed data saw the medians ± range determined for each region. with cortical width measurements having a static 20 measurements per region. All regions were analysed separately including a combined total bone measurement of all regions of the bone image.

Chapter 3.0: Measurement of cortical porosity in the underloaded ovine calcaneus

3.1.1: Introduction

Porosity has been well documented as a parameter for bone loss, as seen in aging (Ferguson, Ayers, Bateman, & Simske, 2003) (Russo, et al., 2006), post-menopausal women (Vilayphiou, Boutroy, Sornay-Rendu, Van Rietbergen, & Chapurlat, 2016) (Riggs, et al., 2004) and disuse osteoporosis/osteopenia (Qin, Lam, Malbari, Shih, & Carroll, 2009) (Gross & Rubin, 1995). Mechanical under-loading and disuse are often used interchangeably to mean a reduction/ absence of mechanical load, likely leading to increased porosity and hence reduced bone strength. An increase in porosity is associated with a similar increase in cortical remodeling (Yerramshetty & Akkus, 2012). As reduced weight bone loss occurs, bone remodeling favours resorption (the osteoclastic response to a reduced load) over formation and a decrease in the deposition of bone occurs (Thomsen, Christensen, Jens Bay Vegger, & Nyengaard, 2012). In turn, greater remodeling and reduced formation within the BMU produces a larger number of resorption lacunae (pores). As they continue to remodel, larger pores connect to smaller pores creating remodeling clusters and increasing overall porosity (Jordan, et al., 2000).

3.2.1: Results: Cortical Porosity

The cortical porosity was analysed at both the level of the whole calcaneus cross-section and by individual anatomical region.

The data of mean percentage cortical porosity (mean +/- standard error [s.e]) are presented in table 1 and figure 16.

Overall (all anatomical regions combined) there were no significant differences in cortical porosity.

Table 1: Mean % cortical porosity at the 3-time points, day 0, week 4 and week 16 (post under-loading by external fixation) for the whole cross-section and the four individual anatomical regions of the ovine calcaneus.

	%porosity									
	Combined regions	Std. Error	Medial	Std. Error	Lateral	Std. Error	Ventral	Std. Error	Dorsal	Std. Error
Day0 (Control)	5.0	0.7	4.9	0.9	3.6	0.9	8.2	1.7	3.5	0.3
Week4	4.0	0.6	3.5	0.7	4.5	1.5	3.7	0.7	4.8	0.7
Week16	5.8	0.5	4.6	0.8	4.3	1.3	9.1	1.3	7.4	1.4

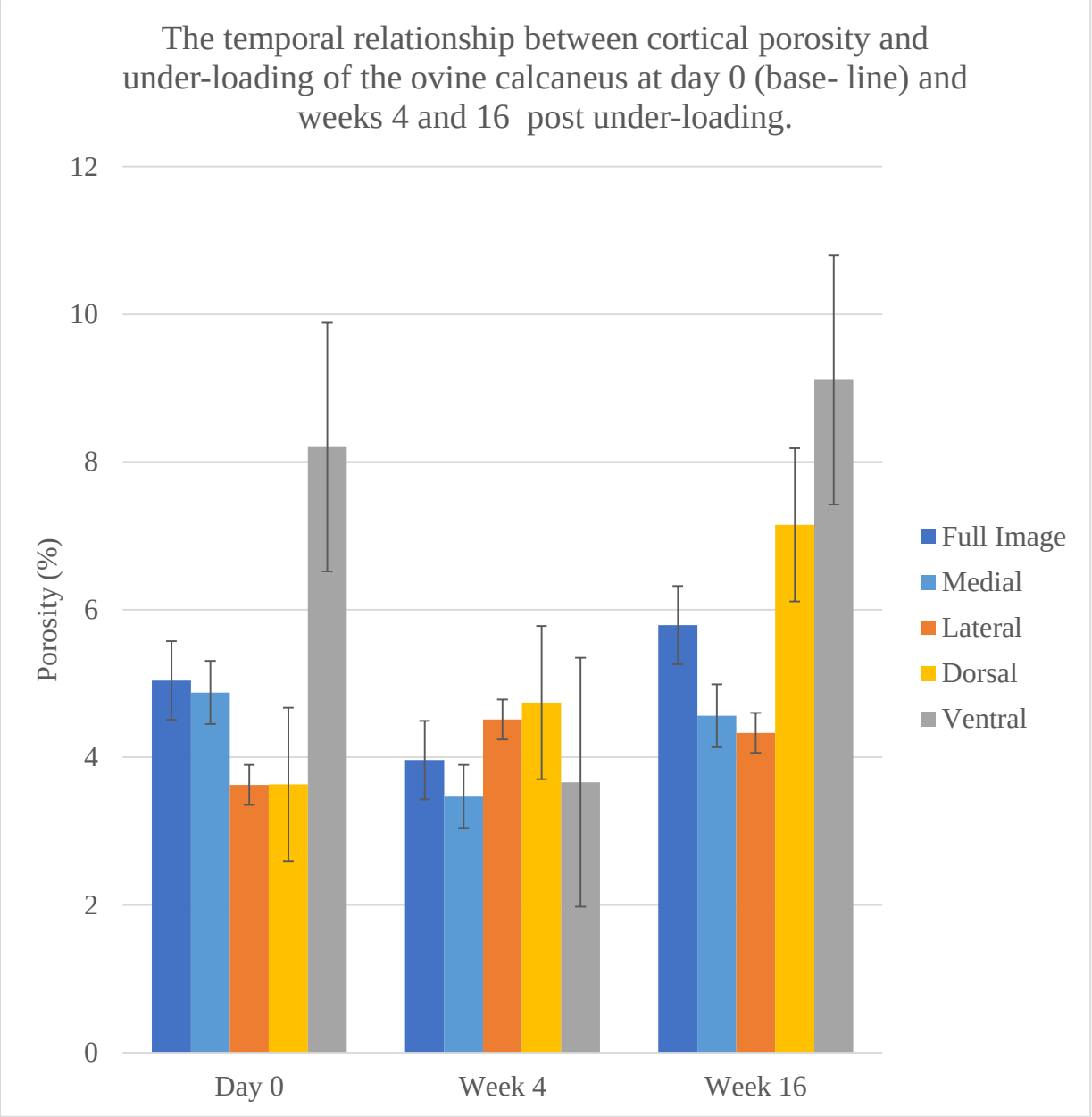

Figure 16: Mean % cortical porosity of whole cross-section and the four anatomical regions(mean +/- s.e) of the underloaded ovine.

When cortical porosity was analysed at a regional level, significant differences were observed between day 0 and the later time points in the ventral and dorsal cortex. With regards to the dorsal region (Figure 17) the porosity was unexpectedly reduced by week 4 (-4.5%) (p=0.028) followed by a significant increase by week 16 (+5.4%) (p=0.018). Porosity between base-line (day 0) and week16 was not however significantly different.

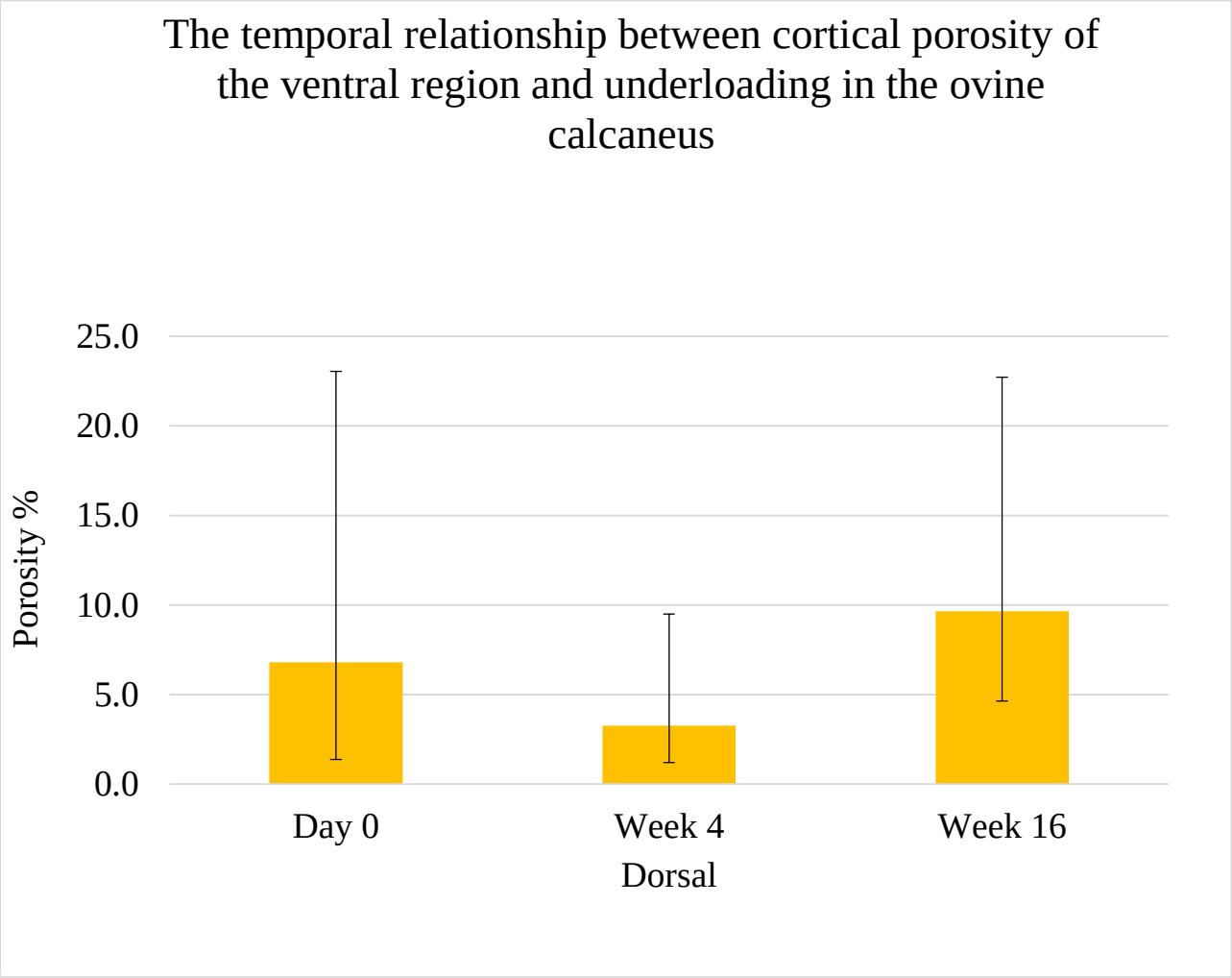

Figure 17: Median cortical porosity of the dorsal cortex in the underloaded ovine calcaneus at day 0 (baseline) and weeks 4 and 16 post under-loading ± range

The cortical porosity in the ventral region (Figure 18) was found to significantly increase (p=0.017) by 4.0% between (3.5%;±0.2) day 0 and week16 (7.4% ±1.4).

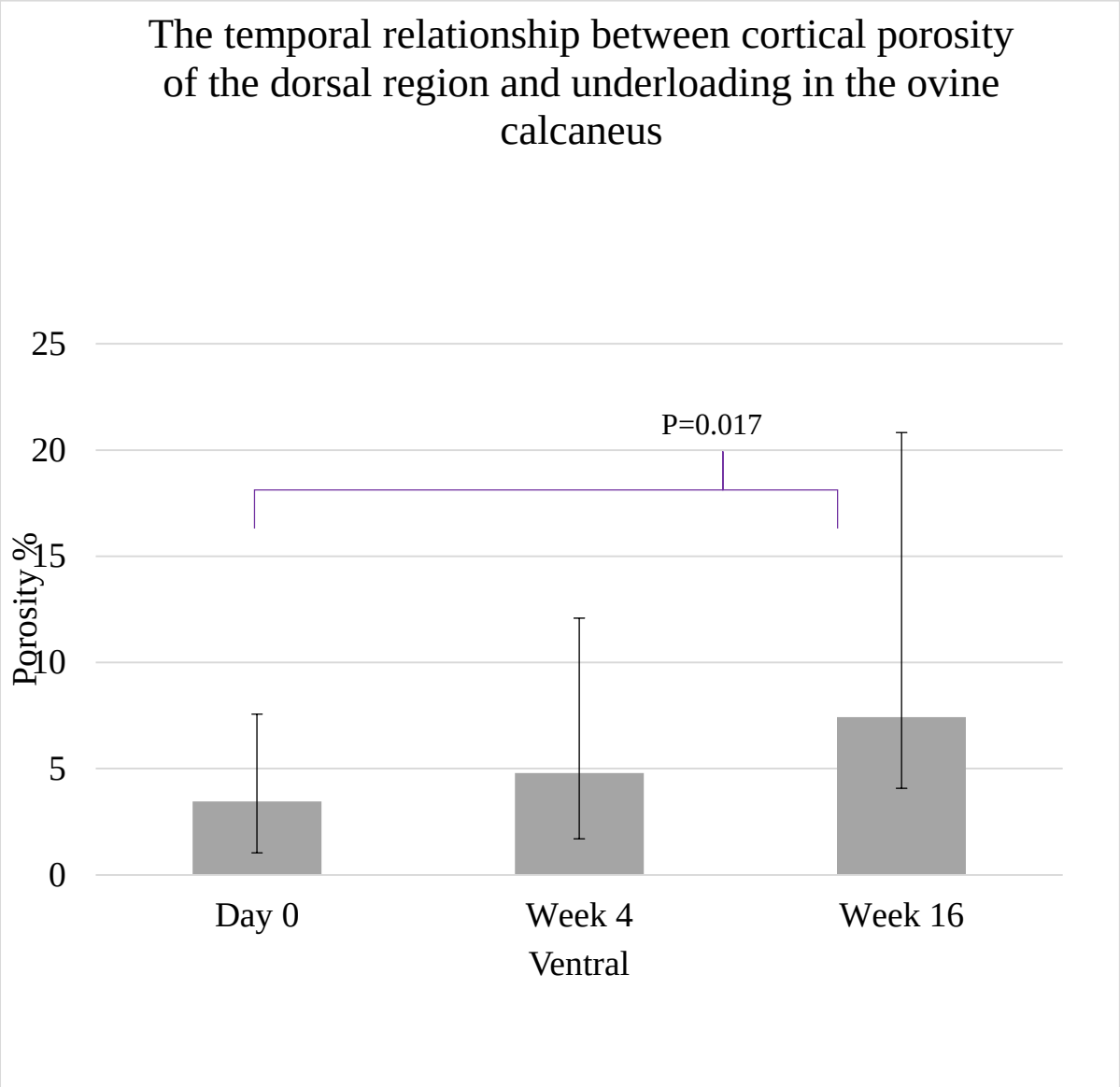

Figure 18: Median cortical porosity of the dorsal cortex of the underloaded ovine calcaneus at day 0 (baseline) and weeks 4 and 16 post under-loading ± range

3.3.1: Discussion

Whilst overall (analysis of the complete cross-section where all regions were combined) there were no significant differences between the cortical porosity of day 0 and the later time points (Figure 19). When analysed regionally, however, significant differences in porosity were detected.

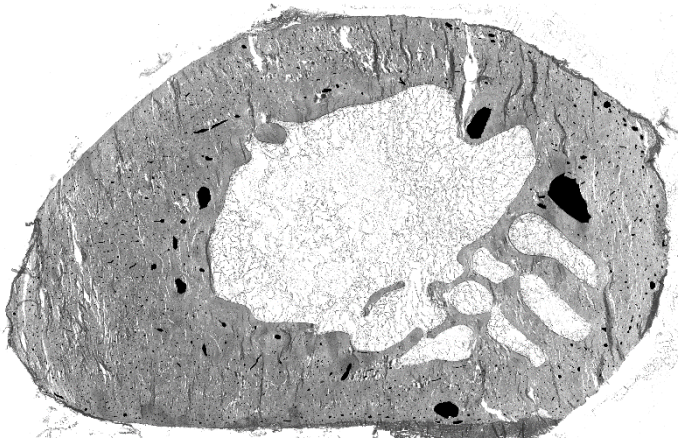

A)

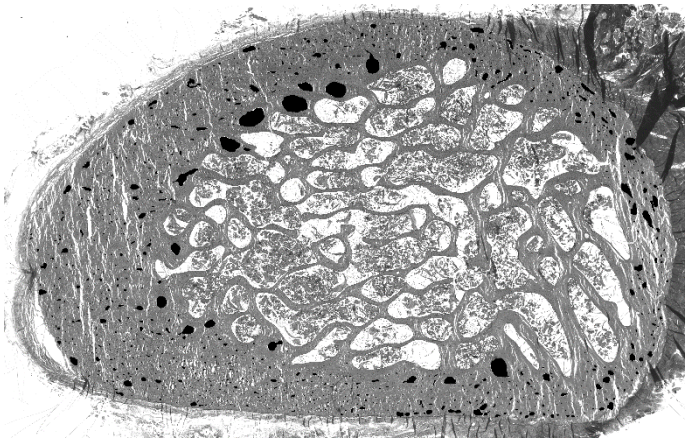

B)

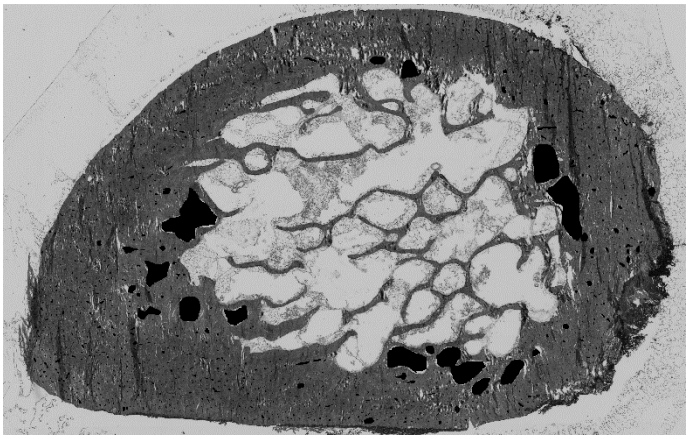

C)

Figure 19: Comparison of cortical porosity between time points (A) Day 0 (B) Week4 (C) Week 16 where total porosity is measured by a black fill of said pores.

In the dorsal region, the porosity was unexpectedly seen to decline between day 0 and week 4. There is no plausible explanation for this finding in terms of its link to the under-loading environment. This decrease in porosity may reflect relatively high inter-subject variation, local to the dorsal region, associated with the relatively small study sample size. The ventral region demonstrated a significant increase in porosity between day 0 and week 16 post under-loading (4.0% increase, $p=0.017$). An explanation for this result can be made by the BMU favouring resorption during periods of low stress in bone (Frost H. M., 1987). Greater porosity has also been associated with larger but less numerous osteons joined with a reduction in cortical infilling (Goldman, Hampson, Guth, Lin, & Jepsen, 2014). Furthermore Bell, et al., (1999) demonstrated both increased porosity ($16.05 \pm 1.8\%$, $p < 0.005$) and increased canal diameter (60 ± 2.8 μm) in the superior region of the underloaded femoral neck (when compared to the inferior region). These findings suggest the change in porosity in the underloaded ovine model was, in part, due to a relatively high porosity when compared to the tension cortex. This effect possibly causes a magnified osteoclastic resorption at the surface of cortical canals. This could therefore lead to larger osteonal formation and a diminished infilling. Although the diminished infilling reduces the area of the cortex within a normally loaded model, bone formation would be encouraged. Any mechanical force applied is more concentrated in the smaller area of the cortex thus triggering an influx of bone

formation (as stated by Wolff's Law). In the ovine under-loaded model investigated here, by week 16, porosity was only observed to be reduced by 4%. This level of reduction, while significant, at this intensity/ duration of under-loading might not be sufficient to induce the structural changes observed by Skedros, Mason, & Bloebaum (1994) within their artiodactyl model.

Jordan, et al., (1998) reported on regional cortical porosity, not in the ovine calcaneus buts its human analogue, the femoral neck. They found in ageing patients that had suffered osteoporotic hip fracture where these subjects might experience conditions of relative skeletal under-loading (arguably not dissimilar to the ovine model investigated here) as a likely factor leading to reduced bone mass. These authors found that the amount of remodelling osteonal clusters per $25mm^2$ was highest within the antero-superior regions at 5.31 (± 1.1) $p = 0.013$. The mean number of clusters per 25 mm^2 per region correlated with the mean porosity per region ($p = 0.014$) Investigating the same anatomic site in humans (the femoral neck), Bell et al, (1999) found the greatest increases in porosity (41%) in the anterior region of hip fracture patients relative to non-fractured controls, although this did not reach statistical significance ($p=0.06$).

Both in the ovine under-loaded calcaneus presented here and the histomorphometric studies based on the osteoporotic human femoral neck show increases in cortical porosity. These increases between the human femoral neck and ovine calcaneus appear however not to be observed in similar anatomical zones experiencing the same habitual loading regimes.

Both Bell et al., (1999) and Jordan (2000) found higher porosity approximating to the cortex loaded in the neutral axis of the fracture patients (i.e. anterior and supero-anterior regions). It was somewhat unexpected that the similarly loaded medial/lateral regions of the ovine calcaneus which are relatively under-loaded (compared to the principal loading axis – dorsal/ ventral) did not demonstrate significant increases in cortical porosity. Overall (all regions combined) there was a trend for increased porosity by week 16 (relative to baseline) however future studies incorporating a greater number of animals would have to be performed to detect a significant effect in this parameter.

It can, however, be stated that some parallels may be drawn between Jordan's (2000) findings of higher porosity observed in the antero-superior region of the fractured femoral neck of humans and the significant increase seen in the ventral region of the sheep calcaneus reported here. A portion of the antero-superior region will have experienced loading patterns of compression (due to partial alignment in the principle loading axis). Relative under-loading in both these different sites might, therefore, drove these

observed increases in porosity. Comparably under-loading of the sheep calcaneus has been found to reduce cortical area and mean canal area, both of which show a strong correlation with an increase in porosity (Loveridge, et al., 2011).Though this research only looks at the calcaneus as a whole and not on a regional basis it is still useful as a comparison. An additional parameter of this study which might be explored further is to examine the relative contribution made to total porosity by a range of different canal diameters for example, as Thomas, et al., (2006) noted that in the cortex of the human femur 81% of changes in porosity could be explained by a change in pore area, where the chief contributor to porosity appears to be driven by the largest pores. Additionally, Bell, et al., (1999) formulated a method of categorising pore size, separated into four categories, normal: 16–82 μm; large: 82–172 μm; extra large: 172–385 μm; giant: >385 μm. Allowing for an examination of the distribution of canal size as well as their mean diameter. For example median canal diameter in the anterior region between the fracture cases and controls were significantly different ($p=0.011$) likewise the highest porosity was also seen in the anterior region expressing a 41% higher porosity than the inferior region ($p < 0.01$) and 57% ($p < 0.05$) higher than the posterior region. Mean canal size was found to be highest within the posterior region (60 ± 2.8 μm) and the proportion of giant canals (>385 μm) was doubled in the anterior region. This study demonstrated that the femoral neck cortex of hip fracture

(osteoporotic patients) is associated with a greater number of giant canals.

There are limitations associated with the current study. Histological analysis, while providing high-resolution imaging, allows analysis of only 2-dimensional data which forms incomplete information relating to a 3-dimensional structure. A less invasive and less time-consuming analysis could be based on two methods of in vivo high-resolution peripheral quantitative computed tomography (HR-pQCT) that have been developed, namely that of threshold-based and density-based methods. Both methods have limitations based on a relatively poor resolution in comparison to the microscopic analysis performed here. Thus resulting in an overestimation of bone porosity from the density-based approach (van Lenthe, et al., 2007) and underestimation of bone porosity in the threshold-based method (Jorgenson, Buie, McErlain, Sandino, & Boyd, 2015). The threshold-based method is the superior method however as it provides structural information, complementing the measure of cortical porosity, for example, the amount of pores and interconnectivity. It is also able to precisely identify the larger pores (above 140 μm in diameter) which are the most relevant to bone biomechanical strength (Jorgenson, Buie, McErlain, Sandino, & Boyd, 2015). The current gold standard for in vivo image analysis is synchrotron radiation micro-computed tomography (SRμCT), this would have produced a higher accuracy, up to 100nm, and shown a

digital 3d image as opposed to the 2d images used in this study. As a technique it has been shown to precisely calculate porosity, surface area, and 3D measures such as strut thickness, pore size, and pore distribution; moreover, it permits precise measurements of bone growth (van Lenthe, et al., 2007).

The application of high-resolution CT might complement the findings presented here through the generation of 3-dimensional imaging leading to more representative data. In addition, this study utilised a manual image analysis methodology, requiring extensive operator man hours. The use of automated computational systems would increase the ability to analyse the number of individual calcaneal cross-sections, thereby making the data more representative at the level of the individual sample.

Chapter 4.0: Changes in cortical width within the underloaded model of the ovine calcaneus

4.1.1: Introduction

Cortical width is a key structural indicator of bone strength. Measurement of this parameter when investigating a difference in bone volume associated with mechanical under-loading is therefore important to quantify. During a period of under-loading on adult female Beagle dogs, cortical area (a similar structural parameter to cortical width) to was reduced (Bloom & Schaffler, 2001). This effect is caused by an increase in cortical remodeling that favours resorption (osteoclast recruitment) and a higher porosity as can be seen in an underloaded model A.) (Bell, et al., 1999) B.) (Bell K.L., 1999). Likewise, within the same underloaded model, cortical thickness reduction was found to correlate with BMU activation frequency rather than the total number of BMU's (He & Ming, 2010). Several other animal models investigating changes in cortical area in response to mechanical load have been researched such as, immobilization in rats (Bagi, Mecham, Weiss, & Miller, 1993) (Izawa, et al., 1981) (Bagi, Miller, Bowman, Blomstrom, & France, 1992), loading of the tibia in aged mice (Brodt & Silva, 2010) and in the ovine model (Loveridge, et al., 2011).

4.2.1: Results: Cortical Width

The mean cortical width (mm) is presented in table 2 and Figure 20. Overall there was a significant reduction in cortical width between day0 (8.1±0.4) and week16 (6.5±0.2), p=0.025. A 19.7% (1.6mm) reduction was observed between those time points. Similarly, cortical width was shown to be reduced by 22.6% between week4 (8.4±0.5) and week16 (6.5±0.2), p=0.028.

Table 2: Mean cortical width (mm) at the 3-time points, day 0, week 4 and week 16 (post under-loading by external fixation) for the whole cross-section and the four individual anatomical regions of the ovine calcaneus.

	Cortical Width (mm)									
	Combined Regions	Std. Error	Medial	Std. Error	Lateral	Std. Error	Ventral	Std. Error	Dorsal	Std. Error
Day0 (Control)	8.1	0.4	2.0	0.0	1.7	0.1	2.9	0.2	1.5	0.1
Week4	8.4	0.5	2.2	0.2	1.6	0.1	3.0	0.1	1.6	0.2
Week16	6.9	0.2	1.7	0.1	1.5	0.0	2.2	0.3	1.5	0.3

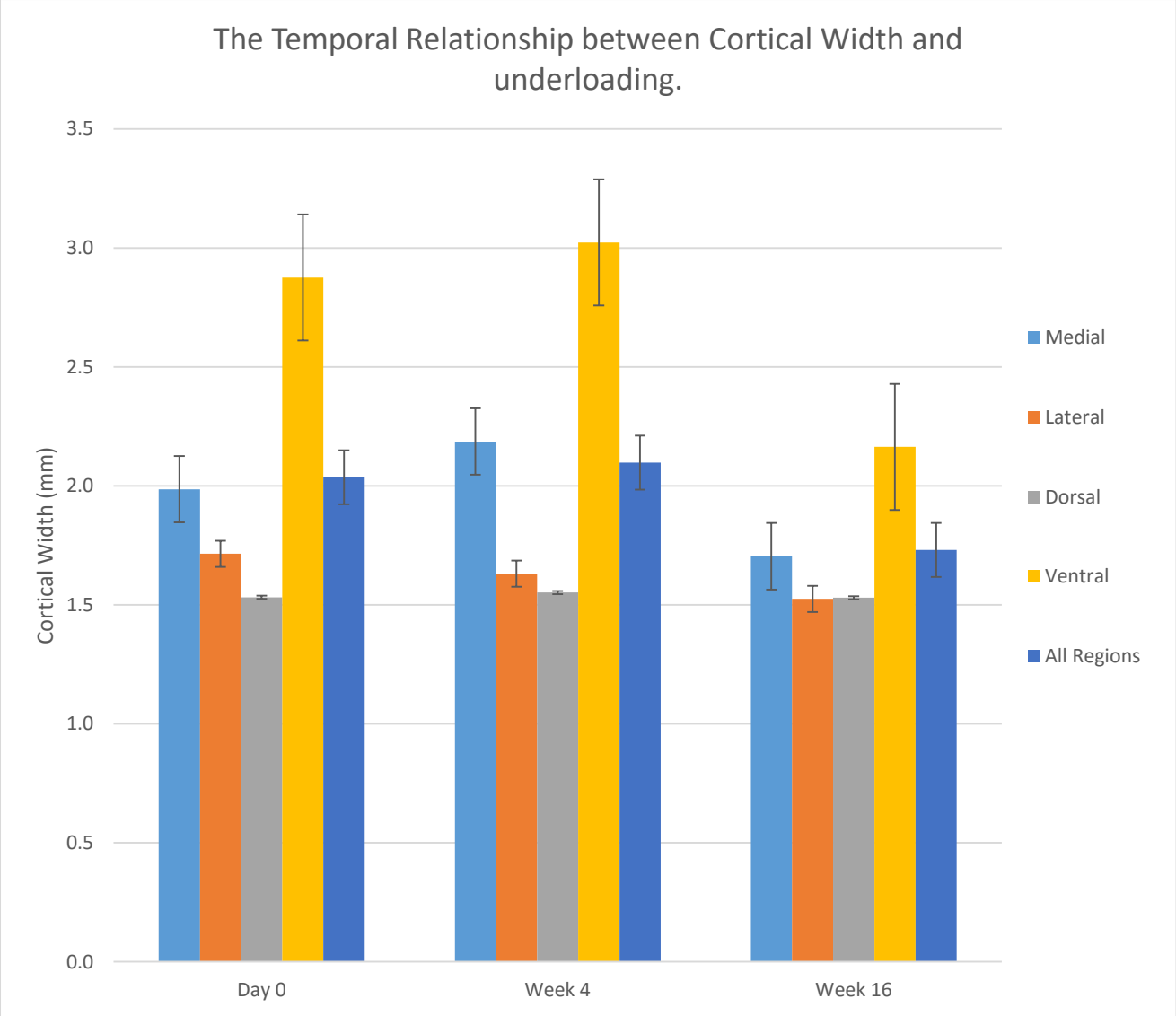

Figure 20: Mean cortical width (mm) of the whole cross-section and the four anatomical regions (mean +/- s.e) of the underloaded ovine.

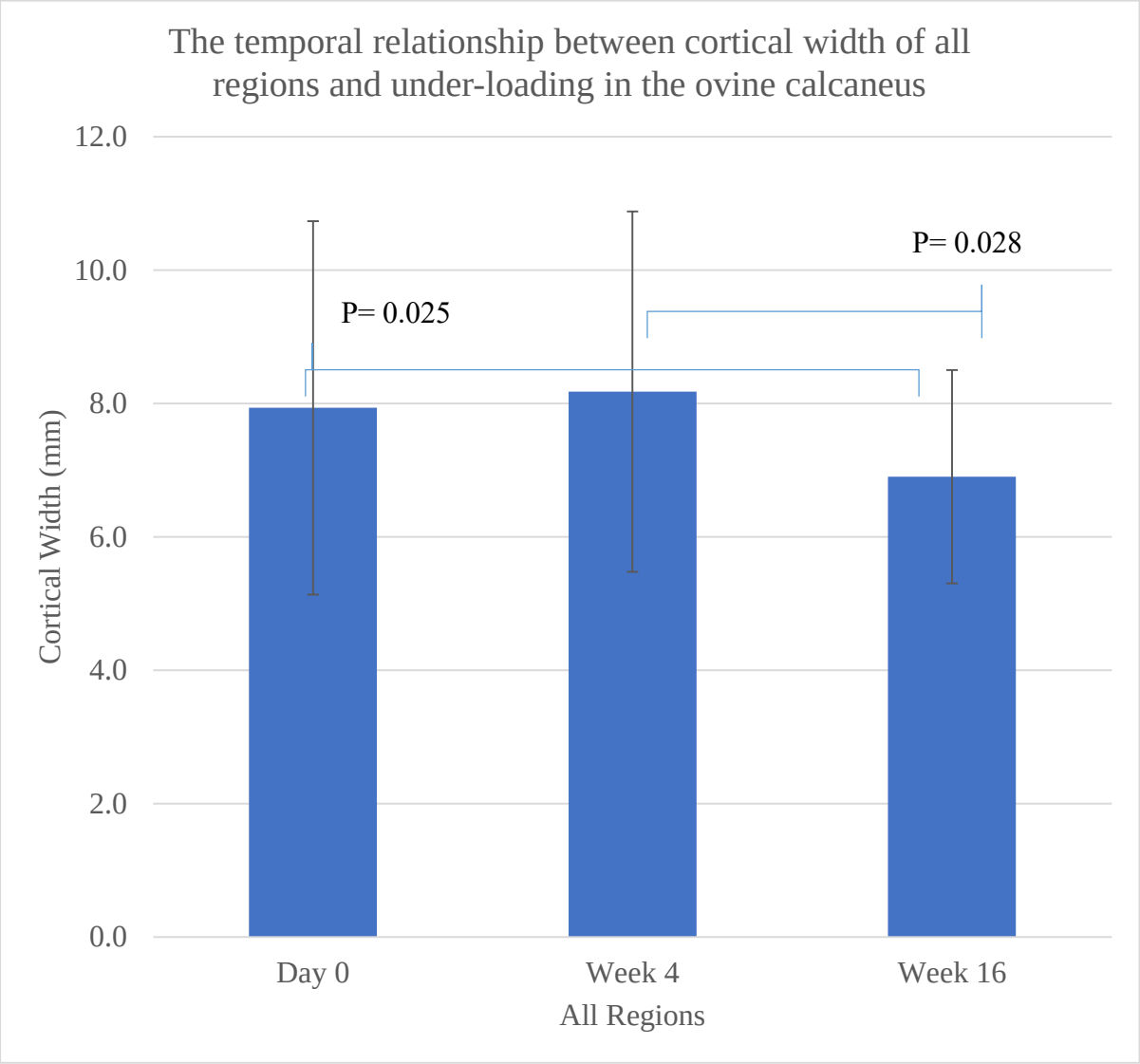

Figure 21: Median cortical width (mm) of all combined regions of the underloaded ovine calcaneus at day 0 (baseline) and weeks 4 and 16 post under-loading ±range

A similar trend can be seen in the ventral region where a reduction in cortical width was observed between day0 (2.9±0.2) and week16 (2.2±0.2) as well as week4 (3.0±0.1) and week16 (2.2±0.2) (figure 22). Though between day0 and week 16 p=0.055, it is close enough to p=0.05 to warrant mentioning. Between the latter time points, a p-value of 0.006 was found. A loss of 23% cortical width was observed between the control and final time point, between week4 and week16 cortical width showed a 26% reduction.

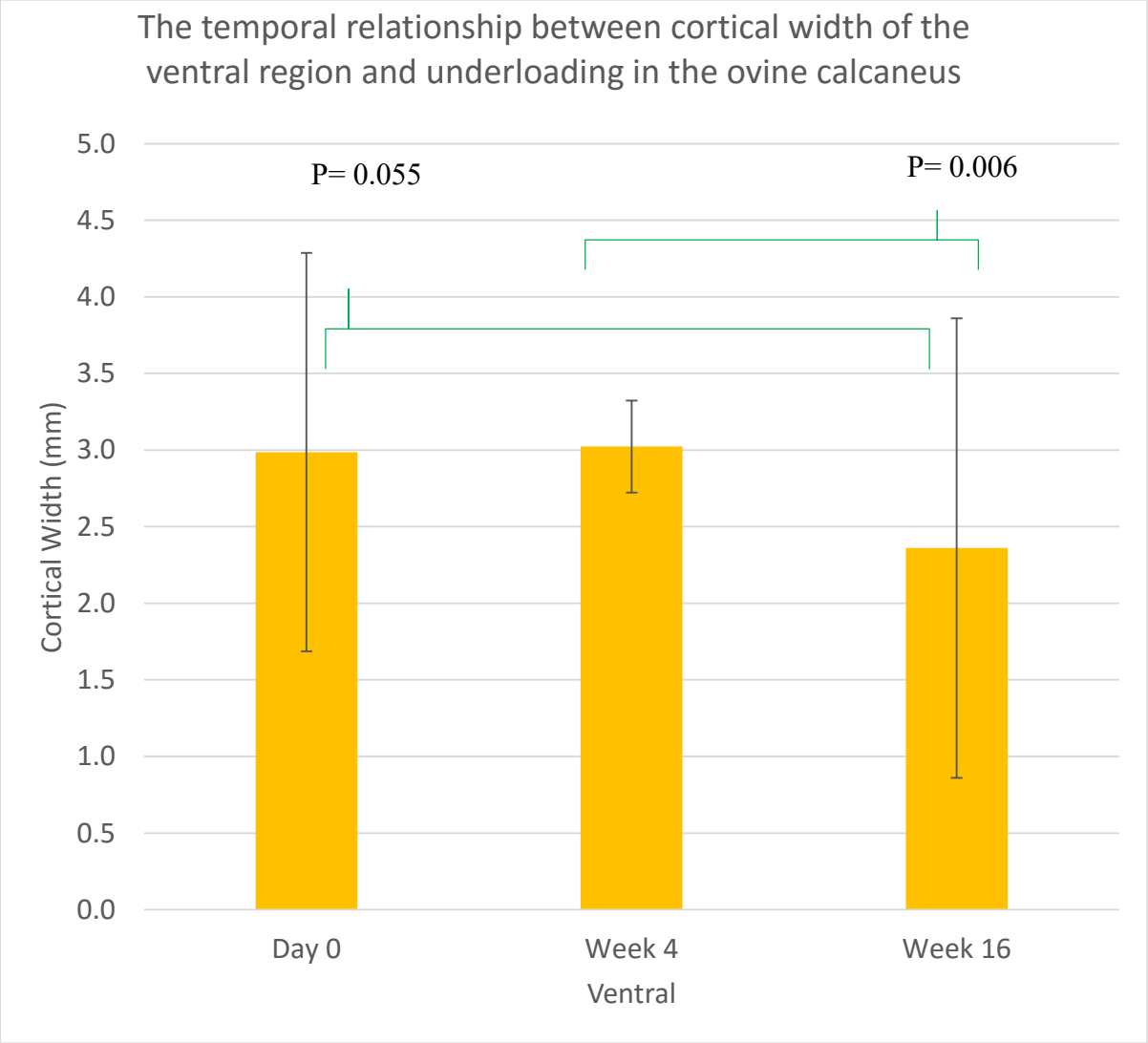

Figure 22: Median cortical width of the ventral cortex of the underloaded ovine calcaneus at day 0 (baseline) and weeks 4 and 16 post under-loading ±range

A significant reduction in cortical width was demonstrated in the medial region between day 0 (2.0±0.0) and week 16 (1.7±0.1), p=0.004, and week 4 (2.2±0.2) and week16 (1.7±0.1), p=0.0028 (figure 23). The net loss of cortical width between the control (day 0) and week 16, and week4 and week16 were 15% and 22% respectively.

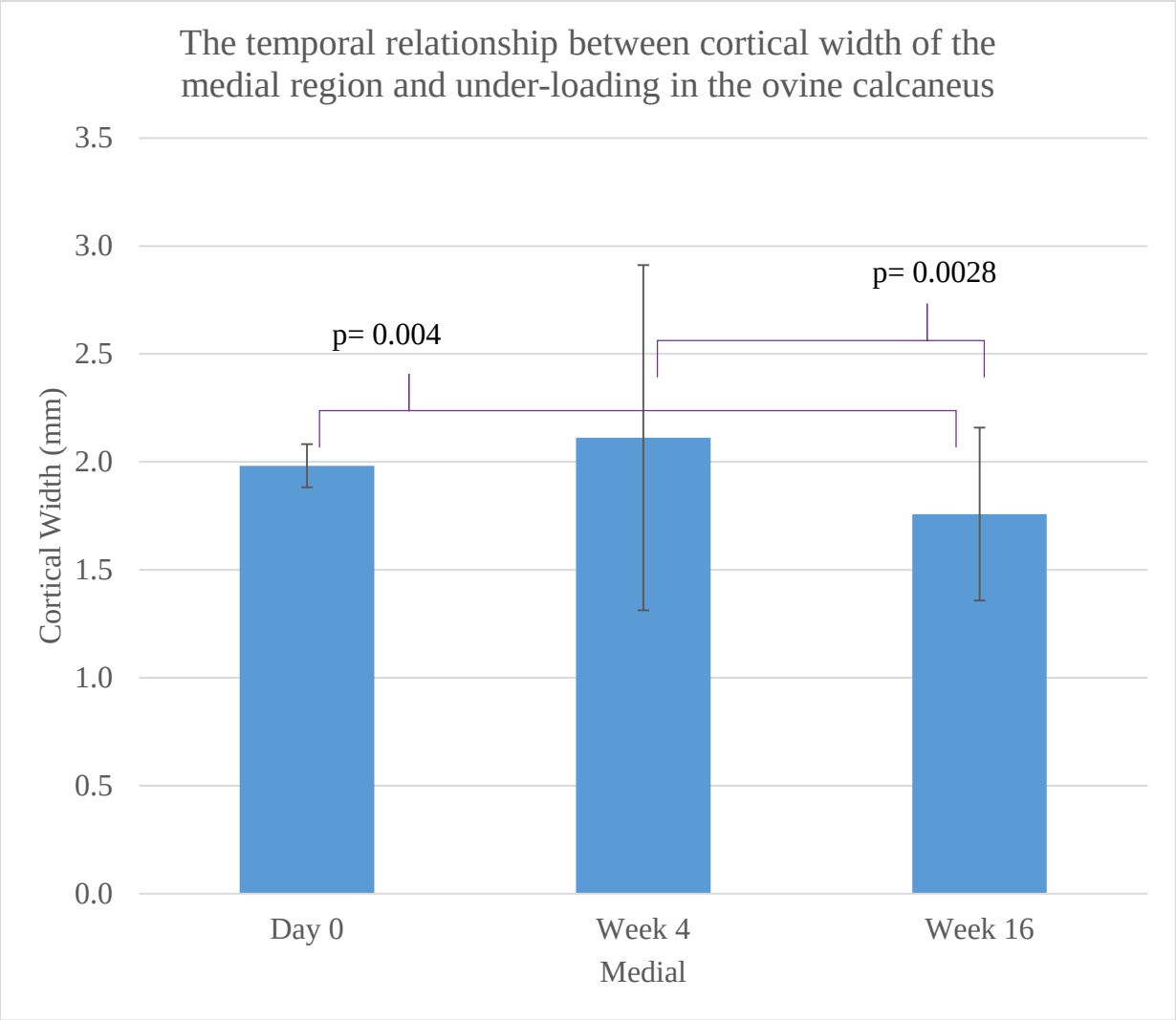

Figure 23: Median cortical width of the medial cortex of the underloaded ovine calcaneus at day 0 (baseline) and weeks 4 and 16 post under-loading ±range

4.3.1: Discussion

Under-loading of the ovine calcaneus in this study showed a marked difference between the cortical width (all anatomic regions combined) 19.7% (1.6mm) p=0.025 being recorded from the control (day 0) to the final timepoint at week 16. An explanation for the decrease in this structural parameter may be due to increased BMU activation rate in favour of osteoclastic resorption on endocortical and intracortical surfaces. BMU activation frequency was found to correlate with a decrease in cortical thickness (He & Ming, 2010). In addition to this, the BMU activation threshold was found to have a strong coupling with mechanical factors such as under-loading (He, Ming , Hao, Dong, & Lin, 2006).

In the current study, within all regions, the cortical width was not significantly different between day 0 and week 4 then decreased between week4 and week 16 (Fig 24). This unexpected maintenance of cortical width between control and week 4 may be due to subject variation between individual sheep.

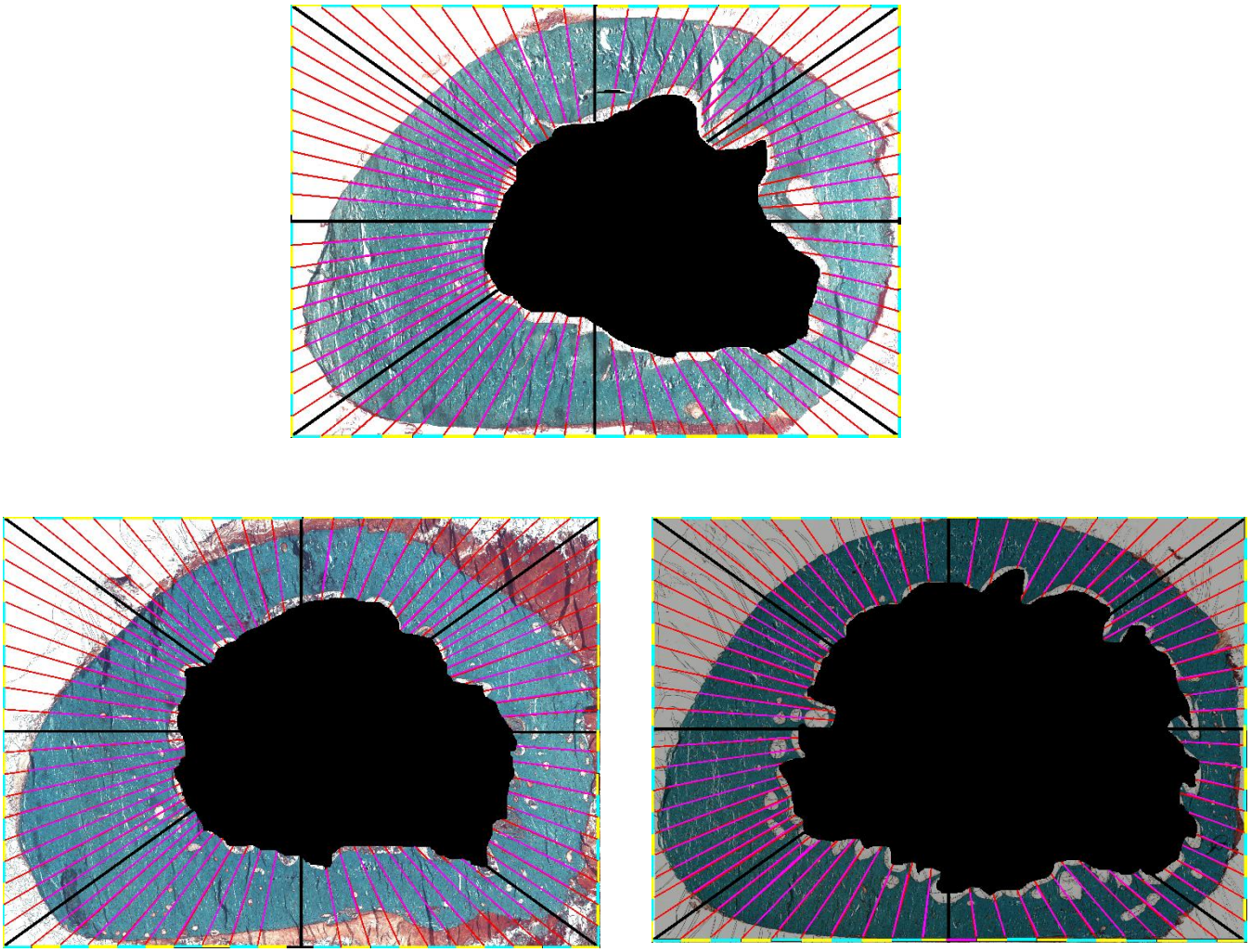

Figure 24. Comparison of cortical width where the blue area shows cortical bone and the pink lines across said cortex denotes a measurement of width. A) Cortical width measurements at day0. B) Cortical width measurements at 4 weeks. C) Cortical width measurements at 16 weeks

Regional reductions in cortical width were observed by week 16 of under-loading. Within the medial region a 15% (p=0.004) loss was seen after 16 weeks, likewise, the ventral region showed a 23%

(p=0.055, borderline significance) reduction in cortical width. Morphologically, as the compression cortex, the ventral region naturally has the thinnest cortical area of other regions before the application of under-loading. Therefore if the same fixed value (in mm) of this parameter was lost in each region this would result in a greater proportional loss of cortical bone width in the ventral region. Additionally, when mechanical stimulation is removed the ventral region is shown to have an acuter resorptive response than that of the neutral or compression axis leading to a 58% increase of the porosity for only 25% of the cortical area (Gross & Rubin, 1995). However in the same study, it was suggested since the expansion of the endosteal envelope was uniform across the cortex, all regions were equally sensitive to disuse, therefore the increased cortical remodeling in certain regions was due to enhanced osteoclast signaling (recruitment and activation). Alternatively, the region in question (i.e the region experiencing the greatest mechanical under-loading) is more accessible to cellular invasion from an increased vascularity. Similarly, Galea, et al., (2015) showed within an aged mouse model of disuse (sciatic neurectomy) a reduction in cortical bone area was site-specific, favouring the proximal (medial and ventral) rather than distal (lateral and dorsal) regions.

Several other animal models have been studied demonstrating similar effects of under-loading on cortical width. Bagi et al,. (1992) found a reduction in cortical area and minimum cortical

width in hindlimb suspended rats. In hindlimb suspended rats an overall reduction in cortical width and expansion of the marrow cavity was observed (Bagi, Mecham, Weiss, & Miller, 1993). Though neither of these examined the same model or bone region they are still useful for analysis. Within the ovine calcaneus in a similar study, Loveridge et al,. (2011) found at 16 weeks the underloaded calcaneus showed a reduced cortical thickness of -0.13mm. This data aligns with the current investigation where total cortical width was reduced by 1.9mm between day0 (control) and week16.

Although the analysis of cortical width in this model did demonstrate significant reductions, an area of improvement in terms of greater representation of data could be achieved through the use of the digital image analysis software, which specifically measures this parameter through calculation of the cross-sectional centre of mass of the bone section (Bell et al., 1999a) . This automated method was developed by Bell, et al., (1995) by which all canals within the bone images were thresholded, this allowed their own image analysis package to set the boundary automatically based on the canals, the boundary was then offset by 150µm to ensure no marrow was included. By using this technique they demonstrated that the highest cortical width was associated with the inferior region whereas the lowest was seen in the superior region of the human femoral neck. This technique was used again to study the structure of femoral neck patients who suffered an

osteoporotic hip fracture. Between the female hip fracture cases and non-fractured, age-matched controls, cortical width was seen to be reduced by 31% in the anterior, inferoanterior region and 25% superoposterior in the fracture group. Within the female osteoporotic group, all regions were lower however only the inferoaterior region showed a significant result of 45.2% reduction in cortical width p=0.0004 (Bell, et al., 1999). Although neither of these image analysis studies are based on an ovine model or investigating the effects of loading, they still represent a robust method of analysis of cortical width which could be applied to the underloaded model of the ovine calcaneus.

Another potential histological method of investigation could be through the use of brightfield and fluorescent microscopy. Using this technique in the hind limb immobilization model of beagle dogs, the mean cortical width was seen to be reduced by 40% (Yang Li, et al., 2005).

An alternative, noninvasive method of analyzing cortical width could be, for example, that of Coutts, et al., (2015) where " in vitro-based radiography intended to replicate the dual-energy X-ray absorptiometry technique" was to determine age and osteoporotic related differences in cortical bone architecture. These authors found cortical thickness was reduced in the superiolateral region of osteoporotic patients, a finding not dissimilar to the reduction seen in the tension cortex reported here.

When calculating the cortical width in the murine model, micro-computed tomography (μCT) can be used to great effect by efficiently providing relatively high resolution, 3-dimensional data. For example, parameters such as cortical area and periosteal surface were determined (Hammond, et al., 2016).

Chapter 5.0: Analysis of cortical remodeling in the underloaded ovine calcaneus

5.1.1: Introduction

Following the rule of Wolff's law, as mechanical loading changes so should the rate of bone remodeling (Mercuri, Daniel, Hecke, & Carvalho, 2016). Therefore as the mechanical load is reduced then remodeling increases (Mosekilde, 1990) (Wang, 2015). Analysis of bone remodeling can be achieved through measurement of the number of remodeling canals within a sample. This is possible because disuse/under-loading encourages, for example, apoptosis of osteocytes within the BMU (Bakker, Klein-Nulend, & Burger, 2004) (Basso & Heersche, 2006) and osteoclastic recruitment (Aguirre, et al., 2006). Therefore the number of remodeling canals should directly correlate (over time) with the length bone spent underloaded and its subsequent bone loss. A count of remodeling canals can be achieved in two ways, the first of which can be a count of resorbing canals and the second would be the quantitation of forming canals, as adopted here. Bone remodeling is a coupled event (Reinhold, 2015) in which the rate of formation increases

with the rate of resorption (resorption preceding formation) (Mohan & Baylink, 1995). Bone loss seen during immobilization or in a state of under-loading can be attributed to an increase in bone remodeling, due to an inbalance favouring resorption (Erben, 2015). Therefore if a rise in forming canals is observed an even greater increase in resorbing canals should be observed. This suggests measurement of the proportion of canals undergoing bone formation provides a strong indication of the scale of remodeling being undertaken in an underloaded model (assuming the phases of remodeling are coupled).

5.2.1: Results: Forming canals

The forming canal count is presented in table 3 and Figure 25. Overall there was no significant change in forming canals between day0 and week 16, although a trend for increased formation (63%) was observed.

Table 3: Mean % forming canals at 3 time points(post under-loading by external fixation) for the whole cross-section and the four individual anatomical regions of the ovine calcaneus.

	% of Forming Canals									
	All Regions Combined	Std. Error	Medial	Std. Error	Lateral	Std. Error	Ventral	Std. Error	Dorsal	Std.Error
Day0	5.5	2.4	3.5	1.6	11.6	7.3	6.2	3.5	5.7	1.3
Week4	3.7	0.7	3.9	0.3	6.0	1.2	2.7	0.5	5.9	1.1
Day16	8.9	2.7	6.2	0.8	9.7	1.3	4.5	0.8	8.0	1.2

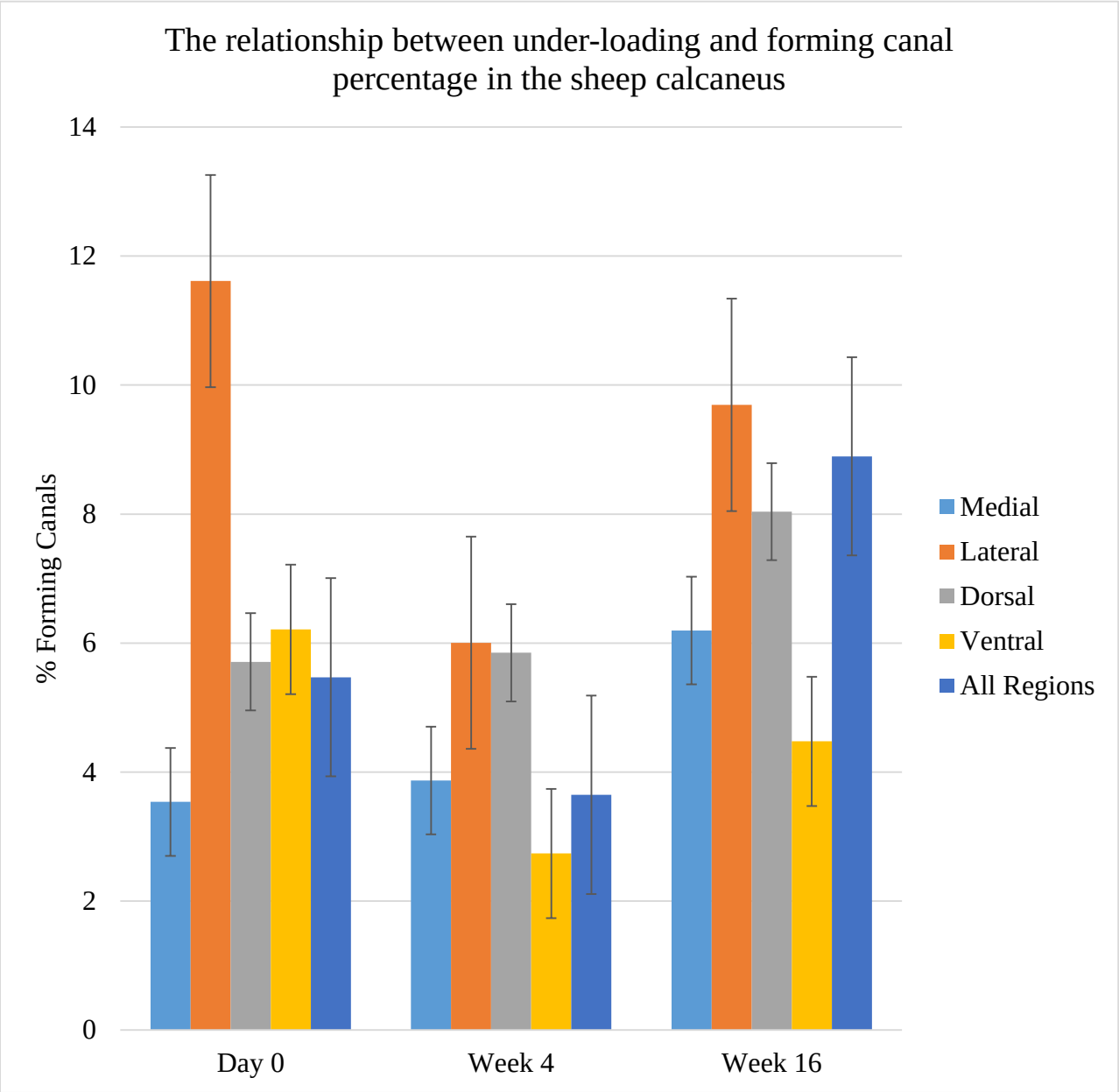

Figure 25: Mean % forming canals of the whole cross-section and the four anatomical regions (mean +/- s.e) of the underloaded ovine.

Only within the medial region could a significant difference in forming canals be observed (Figure 26). Rising by 58% between week 4 (3.9±0.3) and week 16 (6.2±0.8; p=0.028). However between day 0 (3.5±1.6) and week 16 6.2±0.8) a p-value of 0.055 was observed, indicating an increase of borderline significance.

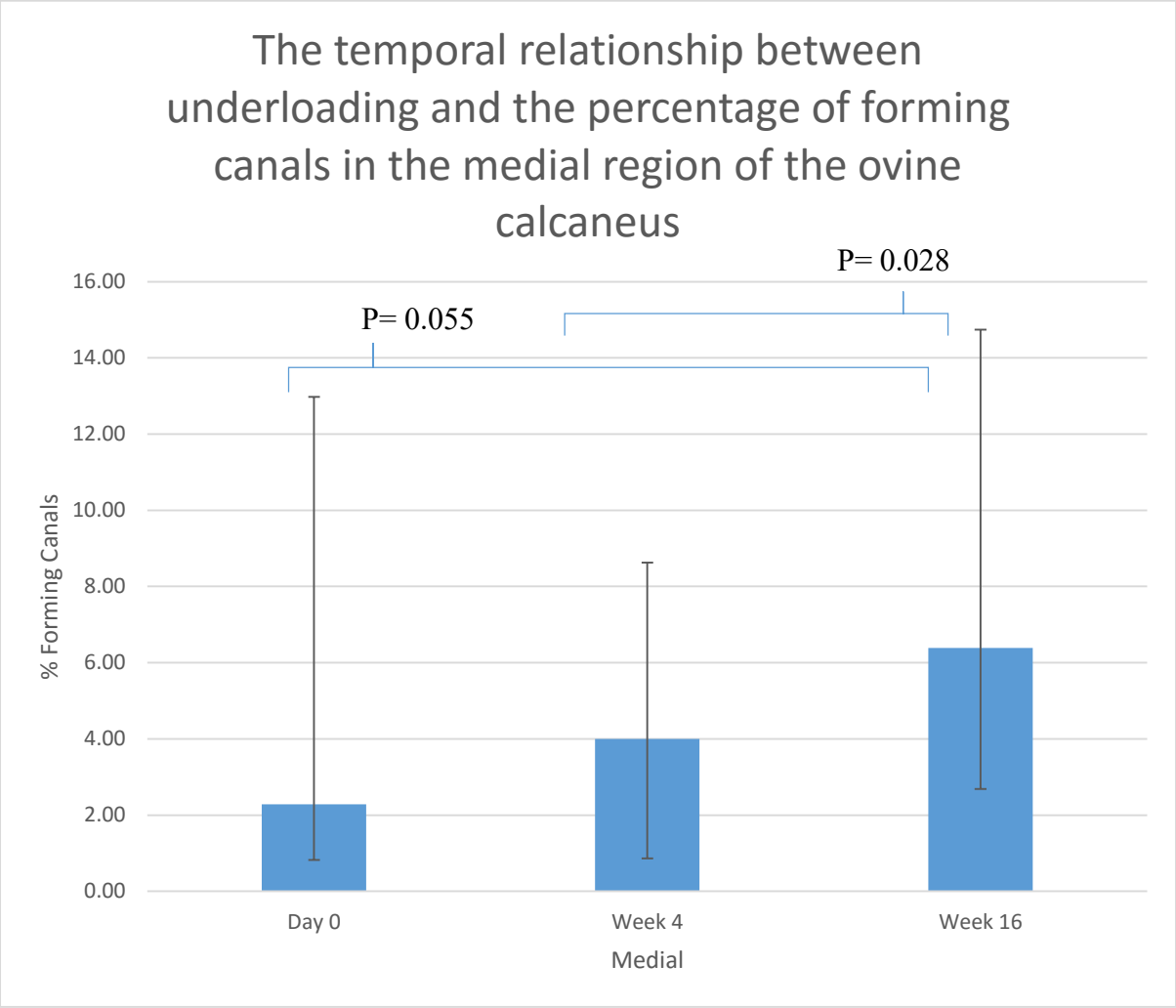

Figure 26: Median % forming canals of the medial region of the underloaded ovine calcaneus at day 0 (baseline) and weeks 4 and 16 post under-loading ± range

5.3.1: Discussion

Overall (all anatomical regions combined) there was a (non-significant) trend for an increase (63%) in the proportion of forming canals by week 16. At the regional level, the principle increase in forming canals could be seen medially between week 4 and week 16, with an increase of 58% ($p=0.028$). Similarly, between the control (day0) and week 16, the proportion of forming canals approached a significant elevation ($p=0.055$) by 77%. These results compare favourably with the findings in the previous chapter namely, that cortical width is reduced within the medial region, therefore, supporting the observation that mechanical under-loading results in a reduced cortical width. Galea, et al., (2015) observed, that the proximal (medial and ventral) region is favoured during remodeling in an aged mouse model of disuse (sciatic neurectomy). Consequently, the findings of increased forming canals within the medial region may be explained by the favouring of this region during remodeling. The number of bone remodeling markers, specifically markers of formation have been shown to increase during periods of under-loading. For example in the “bed rest weightlessness” human model, serum osteocalcin rose one day before the resorption marker hydroxyproline was found to increase. Furthering this osteocalcin remained elevated throughout disuse falling to pre-bed rest after reambulation (Lueken, Arnaud, Taylor, & Baylink, 1993). Similarly Bell (1999a) observed within a hip fracture model of the human femoral neck a reduction in cortical

thickness was attributed to increased cortical remodeling. The proportion of canals undergoing remodeling rose by 56%. Yet the activity of the bone formation markers, tartrate-resistant acid phosphatase (TRAP) and alkaline phosphatase (ALP) increased by similar amounts within the anterior region (55% and 36% respectively). The link between bone formation markers, disuse, and loss of cortical bone is similar to that reported here in the ovine underloaded calcaneus, namely that the number of forming canals increases after 16 weeks of under-loading within the medial region, analogous (in terms of its loading environment) to the anterior femoral neck.

This analysis is not without limitations. A count of resorbing canals would have provided a greater understanding of coupling during remodeling and help to confirm the results gathered in this chapter. In addition to this, a microscopic investigation of regional osteoclastic activity could support results found in this study, namely that mechanical under-loading results in bone loss at a regional level, further verifying the link between under-loading and bone loss in the ovine model.

Immunohistochemical (IHC) analysis would provide a deeper insight into the rate of remodeling, allowing for the comparison of several different markers for bone turnover such as ALP, osteocalcin and TRAP (Dai, Wang, Ang, Yuan, & Koh, 2016) (Siwapituk & Kitisomprayoonkul, 2016) (Čepelak & Čvorišćec, 2009). TRAP also known as acid phosphatase 5 (ACP5) is an iron-

containing enzyme found in humans and is secreted into the blood circulation during bone resorption. TRAP is scarcely detectable in osteoclastic precursors (Alatalo, Halleen, Hentunen, Mönkkönen, & Väänänen, 2000) however during osteoclastogenesis TRAP expression is greatly increased (Oddie, et al., 2000) this in turn allows for the use of TRAP as an IHC marker for bone resorption (Janckila, Takahashi, Sun, & Yam, 2001). Overall a reduction in TRAP overtime is associated with reduced resorptive activity resulting in an osteoporotic phenotype and shortened long bones (Blumer, et al., 2012). Furthering this, mice lacking TRAP exhibited a defect leading to mild osteoporosis (Oddie, et al., 2000) whilst transgenic mice overexpressing TRAP showed a decrease in trabecular bone density with the characteristics of mild osteoporosis (Angel, et al., 2000). In addition in a model of human cell suspension, osteoclasts were found to reduce both TRAP activity and bone resorption when exposed to bisphosphonate drugs or molybdate (Moonga, Moss, Patchell, & Zaidi, 1990). The increase in TRAP expression during osteoclastogenesis is particularly useful when looking at various forms of mechanically loading bone and has been shown numerous times to provide accurate results for example, Kawano, et al., (2001) discovered within the ovariectomized tail suspension model of immobilization (mechanical under-loading) in the femur of rats that after 5 days of immobilization TRAP mRNA levels significantly increased. Loaded limbs also have been seen to have the opposite effect, reducing

TRAP activity of periosteal cells significantly when compared to non-loaded limbs (Henriksen, et al., 2012). These findings indicate a link between TRAP activity, cellular activity, and under-loading.

Another one of these key markers is cathepsin K, it is expressed and then secreted by osteoclasts into bone resorption lacunae for extracellular collagen degradation (Goto, Yamaza, & Tanaka, 2003) (Drake, et al., 1995). Factors that directly moderate osteoclastic bone resorption such as the cytokines, RANKL and TNF-α, and the hormones retinoic acid and estrogen also control cathepsin K gene expression (Troen, 2004). Another cytokine that has a key role in bone resorption is osteoprotegerin ligand (OPGL) was found to cause cathepsin K gene expression. Within histostained bone sections, after reverse transcription polymerase chain reaction (RT-PCR), a blind observer rated the intensity of the stain from 0-3, between the control and 12 hours, 100 ng OPGL treated bone sections, the score for the highest intensity band increased from 2 to 18. This indicates a heightened bone resorption by means of cathepsin K stimulation by OPGL (Corisdeo, Gyda, Zaidi, Moonga, & Troen, 2001). In a study using a Field Emission Scanning Electron Microscope to determine the rate of remodeling caused by overexpression of cathepsin K an increase to osteoclast resorption pit depth and frequency was observed. Osteoclast resorption pit depth differed from 5.99 ± 1.27 µm in the wild-type to 7.86□ ± 0.47 µm. The mean number of resorption pits in osteoclasts were 2.5 ± 0.2 µm2 in the wild-type and 4.5 ± 0.6 µm2 in the cathepsin K

overexpressed type. This indicates a strong correlation between cathepsin K expression and the rate of resorption (Morko, et al., 2009). Sun, et al., (2013) developed an improved method for detecting the active form of cathepsin K, using a highly specific ELISA that detected the N-terminal of only the active and not the pro-form they garnered results of 6.60% and 8.56% variability in means between the intra- and inter-assay respectively. Cathepsin K has been studied very little if at all in the ovine model so whilst there is no research to confirm positive results, it is evident that its expression in relation to bone resorption and therefore presumed link to bone loss in an underloaded model could be quantified through further study.

Chapter 6.0: General Discussion

The aim of the current investigation was to examine the temporal changes (both structural and cellular) associated with mechanical under-loading in the ovine calcaneal model. Using hismorphometric techniques, this experimental system was designed to mimic the biological events associated with disuse osteoporosis and therefore map these changes (over time, i.e. day 0, 4 weeks and 16-week post application of external fixation to the hind limb of sheep) at the tissue/ cellular level.

Within the ovine calcaneus, by week 16 of mechanical under-loading an observed increase in cortical porosity 4%, $p=0.017$ within the ventral region and reduced cortical thickness of 19.7%, $p=0.025$ across all combined regions as well as a regional decrease of 15% and 23% within the medial and ventral regions respectively.

These structural changes coincided with an accompanying increase in cortical remodeling as evidenced by a 58% ($p=0.028$) increase in the proportion of canals undergoing bone formation medially.

Taken together, this data clearly demonstrates the decline in bone mass and increased cellular activity (bone remodeling) associated with a regime of reduced mechanical strain within this skeletal model. Furthermore, the tissue responses to these prevailing conditions of reduced mechanical load appear to mirror the bone loss (and increased bone turnover) ocurring within human subjects suffering from osteoporotic fracture of the femoral neck. This

investigation, therefore, confirms this ovine model as a suitable experimental system to explore in greater detail, (both at the the cellular and molecular levels) the pathological events associated with disuse osteoporosis.

A possible mechanism for the loss of bone seen in this model may be due to an increase in remodeling canals forming giant canal remodeling clusters. Within the model of fracture in the human femoral neck Jordan, et al., (2000) observed a correlation between the mean number of clusters per $25mm^2$ and the mean porosity per region ($p=0.014$). Furthermore the total number of giant canals per region correlated with the total number of remodeling clusters ($p=0.011$). In addition fracture cases when compared to a control saw greater canal clustering per $25mm^2$ within the antero-inferior, antero-superior, and infero-anterior regions. The section outcomes are similar to that found in this study, namely that higher porosity was observed within the ventral (superior) region after 16 weeks as well as the reduction in cortical width combined with the increased cortical remodeling seen medially and are were therefore seen as expected outcomes.

Overall this research has shown that mechanical under-loading does have an effect on several parameters (structural and cellular) within the ovine calcaneus resulting reduced bone mass. This study clearly supports the contention that this model of under-loading is a valid system in which to investigate in greater detail, the cellular and molecular events ocurring in skeletal tissue leading to bone loss.

With a greater sample size reducing the variance within the data, borderline significant data could show more of a significant trend and go towards further affirming the results found in this research.

Heightened porosity associated with a period of under-loading was observed in this study, however, deeper analysis is possible, for example, investigations into remodeling clusters (Jordan, et al., 2000) as well as cortical canal size distribution (Bell, et al., 1999). Analysis of these two perimeters could help distinguish if the bone loss seen in this study is further linked to rising porosity namely that remodeling clusters form larger pores with a greater canal size driving regional porosity. Additionally the use of this model could help confirm other findings such as changes in the osteocyte network in response to mechanical load, within the femur of the temporal newly born mouse model osteocyte network formation was shown to increase after 6 weeks of mechanical loading (Sugawara, et al., 2013), suggesting a link between them. Insight into the changes experienced by the osteocyte network within the underloaded ovine model would help towards confirming the mechanisms behind bone loss such as increased osteocyte connectivity or density, what effect changes in the osteocyte network have on cortical porosity and it's influence on the rate of remodeling. Furthering this osteocyte apoptosis could be used as a parameter for bone loss, specifically, it's effect on the osteocyte network. A computer simulated 5% increase in apoptotic osteocytes was found to decrease mean signaling levels between the osteocyte

network and the bone lining cells by 25% (Jahani, Genever, Patton, Ahwal, & Fagan, 2012). This reduced signaling inhibits the ability of bone to respond to microdamage and therefore leads to an increase in skeletal fragility. Expanding on the relationship between osteocyte apoptosis and bone loss, within the avian ulna model of disuse osteopenia Dodd, Raleigh, & Gross., (1999) found osteocyte hypoxia significantly increased 8.4 +/- 1.8% after 24 hours of unloading. Likewise, Cabahug-Zuckerman, et al., (2016) detected a 4 fold increase in osteocyte apoptosis after 5 days of hindlimb unloading the femurs of mice corresponding with a similar increase in the number of osteocytes producing the cytokine and key bone receptor activator RANKL. Both of these studies are performed within an underloaded model, therefore, a similar response (under-loading causing osteocyte apoptosis, therefore, encouraging production of bone remodeling markers) can be expected within the underloaded ovine model. RANKL expression within an unloaded mouse model was found to increase however inhibition of osteocytic apoptosis did not hinder osteoclastogenesis or prevent further resorption (Plotkin, et al., 2015). Future study of biochemical markers of bone resorption (i.e. pyridinium crosslinks, collagen I C- and N-terminal telopeptides) (Camozzi, et al., 2007) could help provide an understanding of the mechanisms by which under-loading results in resorption.

Immunohistochemical staining of biochemical bone markers would provide a greater understanding of cellular activity within the underloaded model of the ovine calcaneus. For example, a marker for osteoblast migration (Sheu, et al., 2003) and osteoclast activity (Ballanti, et al., 1997) TRAP, has been found to show increased expression in multinucleated cells of the tail-suspended mouse model after a period of 1 week of under-loading, rising significantly higher after 2 weeks (Sakai & Nakamura, 2001). Similarly, within the ovariectomized tail suspension model of immobilization in the femur of rats, 5 days after immobilization TRAP mRNA levels significantly increased (Kawano, et al., 2001). Expanding on this, TRAP levels could provide an indicator of regional osteocyte density as it's located on RANKL/OPG-positive secretory lysosomes in osteoblasts and osteocytes (Solberg, Stang, Brorson, Andersson, & Reinholt, 2014). For example within the unloaded model of the tibial diaphysis of the rat osteocyte lacunar density was significantly reduced in immobilized bones (49,642 ± 11,955 lacunae per mm^3) when compared to controls (63,138 ±1956 lacunae per mm^3), $p<0.05$ (Britz, et al., 2012). Adapting these methods and applying them to an ovine model of under-loading may provide insight into any correlation between osteocyte densities, mean canal size and remodeling clusters in response to under-loading if analysed together.

ALP is an enzyme histochemical marker for bone formation linked to remodeling, within the hip fracture model of the femoral neck

regional increases of 36% were observed along with a concurrent rise of 56% in remodeling activity within the anterior (medial) region (Bell K.L., 1999). Additionally within the hind-limb suspension model of rat tibial bone after 5 days of suspension a 61% increased expression of ALP was detected (Kostenuik, Halloran, Morey-Holton, & Bikle, 1997), highlighting possible further correlation between the bone loss seen in the underloaded model of the ovine calcaneus and concentrations of the bone formation marker ALP.

Overall there are numerous avenues to explore in regards to further application of the data gathered within this study. It is evident that the underloaded model of the ovine calcaneus has the potential to be a crucial model in assessing the effects of under-loading on bone. It's likeness to the human femoral neck (similar structure) allows for research of the ovine calcaneus to be used as a template for femoral neck research and most critically a greater understanding of the function and mechanisms involved with bone remodeling.

Chapter 7.0: References

Adler, R. A. (2013). Osteoporosis in men: recent progress. *Endocrine*, *44*(1), 40-46.

Aguirre, J. I., Plotkin, L. I., Stewart, S. A., Weinstein, R. S., Parfitt, A. M., Manolagas, S. C., & Bellido, PhD, T. (2006). Osteocyte Apoptosis Is Induced by Weightlessness in Mice and Precedes Osteoclast Recruitment and Bone Loss. *Journal of Bone and Mineral Research*, *21*(4), 605–615.

Alatalo, S. L., Halleen, J. M., Hentunen, T. A., Mönkkönen, J., & Väänänen, H. K. (2000). Rapid Screening Method for Osteoclast Differentiation in Vitro That Measures Tartrate-resistant Acid Phosphatase 5b Activity Secreted into the Culture Medium. *Clinical Chemistry, 46*(11), 1751-1754.

Angel, N. Z., Walsh, N., Forwood, M. R., Ostrowski, M. C., Cassady, A. I., & Hume, D. A. (2000). Transgenic Mice Overexpressing Tartrate-Resistant Acid Phosphatase Exhibit an Increased Rate of Bone Turnover. *Journal of Bone and Mineral Research, 15*(1), 103-110.

Arden, N. (2006). *Osteoporosis* (2 ed.). Remedica.

Bagi, C. M., Mecham, M., Weiss, J., & Miller, S. C. (1993). Comparative morphometric changes in rat cortical bone following ovariectomy and/or immobilization. *Bone, 14*(6), 877-883.

Bagi, C. M., Miller, S. C., Bowman, B. M., Blomstrom, G. L., & France, E. P. (1992). Differences in cortical bone in overloaded and underloaded femurs from ovariectomized rats: comparison of bone morphometry with torsional testing. *Bone, 13*(1), 35-40.

Bakker, A., Klein-Nulend, J., & Burger, E. (2004). Shear stress inhibits while disuse promotes osteocyte apoptosis. *Biochemical and Biophysical Research Communications, 320*(4), 1163–1168.

Ballanti, P., Minisola, S., Pacitti, M. T., Scarnecchia, L., Rosso, R., Mazzuoli, G. F., & Bonucci, E. (1997). Tartrate-resistant acid phosphate activity as osteoclastic marker: sensitivity of cytochemical assessment and serum assay in comparison with standardized osteoclast histomorphometry. *Osteoporosis International, 7*(1), 39-43.

Baohua, J., & Huajian, G. (2004). Mechanical properties of nanostructure of biological materials. *Journal of the Mechanics and Physics of Solids, 52*(9), 1963–1990.

Barak, M. M., Lieberman, D. E., & Hublin, J.-J. (2011). A Wolff in sheep's clothing: Trabecular bone adaptation in response to changes in joint loading orientation. *Bone, 49*(6), 1141–1151.

Basso, N., & Heersche, J. N. (2006). Effects of hind limb unloading and reloading on nitric oxide synthase expression and apoptosis of osteocytes and chondrocytes. *Bone, 39*(4), 807–814.

Bateman, T. A., Dunstan, C. R., Ferguson, V. L., Lacey, D. L., Ayers, R. A., & Simske, J. (2000). Osteoprotegerin mitigates tail suspension-induced osteopenia. *Bone, 26*(5), 443–449.

Bell K.L., L. N. (1999). Intracapsular hip fracture: increased cortical remodeling in the thinned and porous anterior region of the femoral neck. *Osteoporosis International, 10*(3), 248-57.

Bell, K. L., Garrahan, N., Kneissel, M., Loveridge, N., Grau, E., Stanton, M., & Reeve, J. (1995). Cortical and cancellous bone in the human femoral neck: Evaluation of an interactive image analysis system. *Bone, 19*(5), 541-548.

Bell, K. L., Loveridge, N., Power, J., Garrahan, N., Meggitt, B. F., & Reeve, J. (1999). Regional differences in cortical porosity in the fractured femoral neck. *Bone, 24*(1), 57–64.

Bell, K. L., Loveridge, N., Power, J., Garrahan, N., Stanton, M., Lunt, M., . . . Reeve, J. (1999). Structure of the Femoral Neck in Hip Fracture: Cortical Bone Loss in the Inferoanterior to Superoposterior Axis. *Journal of Bone and Mineral Research,* 111-119.

Bell, K. L., Loveridge, N., Power, J., Garrahan, N., Stanton, M., Lunt, M., . . . Reeve, J. (1999). Structure of the Femoral Neck in Hip Fracture: Cortical Bone Loss in the Inferoanterior to Superoposterior Axis. *Journal of Bone and Mineral Research, 14*(1), 111–119.

Belo, J. N., Berger, M. Y., Reijman, M., Koes, B. W., & Bierma-Zeinstra, S. M. (2007). Prognostic factors of progression of osteoarthritis of the knee: A systematic review of observational studies. *Arthritis Care & Research, 57*(1), 13-26.

Blain, H., Chavassieux, P., Portero-Muzy, N., Bonnel, F., Canovas, F., Chammas, M., & Maury, P. (2008). Cortical and trabecular bone distribution in the femoral neck in osteoporosis and osteoarthritis. *Bone, 43*(5), 862–868.

Bloom, T., & Schaffler, M. B. (2001). *Adult Cortical Bone Recovers from Long-Term Disuse Osteoporosis by Changing Architecture.* Mount Sinai School of Medicine, Department of Orthopaedics. San Francisco: Orthopaedic Research Society.

Blumer, M. J., Hausott, B., Schwarzer, C., Hayman, A. R., Stempel, J., & Fritsch, H. (2012). Role of tartrate-resistant acid phosphatase (TRAP) in long bone development. *Mechanisms of Development, 5-8*(129), 162–176.

Bonewald, L. F. (2011). The amazing osteocyte. *Journal of Bone and Mineral Research, 26*(2), 229–238.

Bonnet, N., Conway, S. J., & Ferrari, S. L. (2012). Regulation of beta catenin signaling and parathyroid hormone anabolic effects in bone by the matricellular protein periostin. *Proceedings of the National Academy of Sciences of the Unnited States of America, 109*(37), 15048–15053.

Braith, R. W., Magyari, P. M., Fulton, M. N., Aranda Jr., J., Walker, T., & Hill, J. A. (2003). Resistance exercise training and alendronate reverse Glucocorticoid-Induced osteoporosis in heart transplant recipients. *The Journal of Heart and Lung Transplantation, 22*(10), 1082–1090.

Britannica, T. E. (2012, February). *Ewing tumour of bone*. Retrieved from Encyclopaedia Brittanica: https://www.britannica.com/science/Ewing-tumor-of-bone

Britz, H. M., Carter, Y., Jokihaara, J., Leppänen, O. V., Järvinen, T. L., Belev, G., & Cooper, D. M. (2012). Prolonged unloading in growing rats reduces cortical osteocyte lacunar density and volume in the distal tibia. *Bone, 51*(5), 913–919.

Brodt, M. D., & Silva, M. J. (2010). Aged mice have enhanced endocortical response and normal periosteal response compared with young-adult mice following 1 week of axial tibial compression. *The Journal of Bone and Mineral Research, 25*(9), 2006–2015.

Brömme, D., & Okamoto, K. (1995). Human Cathepsin O2, a Novel Cysteine Protease Highly Expressed in Osteoclastomas and Ovary Molecular Cloning, Sequencing and Tissue Distribution. *Biological Chemistry, 376*(6), 379-384.

Brown, J. P., Delmas, P. D., & Arlot, M. (1987). Active Bone Turnover of the Cortico-Endosteal Envelope in Postmenopausal Osteoporosis. *The Journal of Clinical Endocrinology & Metabolism, 64*(5).

Buenzli, P. R., Jeon, J., Pivonka, P., Smith, D. W., & Cummings, P. T. (2012). Investigation of bone resorption within a cortical basic multicellular unit using a lattice-based computational model. *Bone, 50*(1), 378–389.

Buenzli, P. R., Pivonka, P., & Smith, D. W. (2011). Spatio-temporal structure of cell distribution in cortical Bone Multicellular Units: A mathematical model. *Bone, 48*(4), 918–926.

Burr, D. B., Forwood, M. R., Fyhrie, D. P., Martin, R. B., Schaffler, M. B., & Turner, C. H. (1997). Bone Microdamage and Skeletal Fragility in Osteoporotic and Stress Fractures. *Journal of Bone and Mineral Research, 12*(1), 6–15.

Cabahug-Zuckerman, P., Frikha-Benayed, D., Majeska, R. J., Tuthill, A., Yakar, S., Judex, S., & Schaffler, M. B. (2016). Osteocyte Apoptosis Caused by Hindlimb Unloading is Required to Trigger Osteocyte RANKL Production and Subsequent Resorption of Cortical and Trabecular Bone in Mice Femurs. *Journal of Bone and Mineral Research, 31*(7), 1356–1365.

Camozzi, V., Tossi, A., Simoni, E., Pagani, F., Francucci, C. M., & Moro, L. (2007). Role of biochemical markers of bone remodeling in clinical practice. *Journal of Endocrinological Investigation, 30*, 13-7.

Canalis, E., Mazziotti, G., Giustina, A., & Bilezikian, J. P. (2007). Glucocorticoid-induced osteoporosis: pathophysiology and therapy. *Osteoporosis International, 18*(10), 1319-1328.

Carpentier, V. T., Wong, J., Yeap, Y., Gan, C., Sutton-Smith, P., Badiei, A., . . . Kuliwaba, J. S. (2012). Increased proportion of hypermineralized osteocyte lacunae in osteoporotic and osteoarthritic human trabecular bone: Implications for bone remodeling. *Bone, 50*(3), 688–694.

Carter, Y., Thomas, C. D., Clement, J. G., & Cooper, D. M. (2013). Femoral osteocyte lacunar density, volume and morphology in women across the lifespan. *Journal of Structural Biology, 183*(3), 519–526.

Carter, Y., Thomas, C. D., Clement, J. G., Peele, A. G., Hannah, K., & Cooper, D. M. (2013). Variation in osteocyte lacunar morphology and density in the human femur — a synchrotron radiation micro-CT study. *Bone, 52*(1), 126–132.

Centers for Disease Control and Prevention. (2003). Trends in Aging -- United States and Worldwide . *Morbitity and Mortality Weekly Report*, 101-104.

Čepelak, I., & Čvorišćec, D. (2009). Biochemical markers of bone remodeling – review. *Biochemia Medica, 19*(1), 17-35.

Childhood Acute Myeloid Leukemia/Other Myeloid Malignancies Treatment (PDQ®)–Patient Version. (2016, February). Retrieved from Nation Cancer Institute:

http://www.cancer.gov/types/leukemia/patient/child-aml-treatment-pdq?utm_content=sf27145602&utm_medium=spredfast&utm_source=facebook&utm_campaign=National%20Cancer%20Institute&cid=sf27145602

Christiansen, P. (2001). Chapter 3: BASIC BONE BIOLOGY. *APMIS, 109*(S102), 6–9.

Coetzee, M., Haag, M., & Kruger, M. C. (2007). Effects of arachidonic acid, docosahexaenoic acid, prostaglandin E2 and parathyroid hormone on osteoprotegerin and RANKL secretion by MC3T3-E1 osteoblast-like cells. *The Journal of Nutritional Biochemistry, 18*(1), 54–63.

Collins, M. T. (2015, June). *Fibrous Dysplasia Overview*. Retrieved from NIH Osteoporosis and Related Bone Diseases National Resource Center: http://www.niams.nih.gov/Health_Info/Bone/Additional_Bone_Topics/fibrous_dysplasia.asp

Corisdeo, S., Gyda, M., Zaidi, M., Moonga, B. S., & Troen, B. R. (2001). New Insights into the Regulation of Cathepsin K Gene. *Biochemical and Biophysical Research Communications, 285*(2), 335-339.

Coutts, L. V., Jenkins, T., Oreffo, R. O., Dunlop, D. G., Cooper, C., Harvey, N. C., & Thurner, P. J. (2015). Local Variation in Femoral Neck Cortical Bone: In Vitro Measured Bone Mineral Density, Geometry and Mechanical Properties. *Journal of Clinical Densitometry*.

Dai, Z., Wang, R., Ang, L.-W., Yuan, J.-M., & Koh, W.-P. (2016). Bone turnover biomarkers and risk of osteoporotic hip fracture in an Asian population. *Bone, 83*, 171–177.

Dallas, S. L., Prideaux, M., & Bonewald, L. F. (2013). The Osteocyte: An Endocrine Cell … and More. *Endocrine Reviews, 34*(5), 658-690.

Damjanov, I. (2000). *Pathology for the health-related professions.* Philadelphia: Saunders.

Dodd, J. S., Raleigh, J. A., & Gross, T. S. (1999). Osteocyte hypoxia: a novel mechanotransduction pathway. *The American Journal of Physiology: Cell Physiology, 277*(3), C598-602.

Doherty, P., & Rahman, P. (2012, November). *What is osteoarthritis?* Retrieved from Arthritis Research UK: http://www.arthritisresearchuk.org/arthritis-information/conditions/osteoarthritis/what-is-osteoarthritis.aspx

Drake, F. H., Dodds, R. A., James, I. E., Connor, J. R., Debouck, C., Richardson, S., . . . Gowen, M. (1995). Cathepsin K, but Not Cathepsins B, L, or S, Is Abundantly Expressed in Human Osteoclasts. *The Journal of Biological Chemistry, 271*(21), 12511–12516.

Erben, R. G. (2015). Hypothesis: Coupling between Resorption and Formation in Cancellous bone Remodeling is a Mechanically Controlled Event. *Fronteirs in Endocrinology, 6*.

Felson, D. T., Zhang, Y., Anthony, J. M., Naimark, A., & Anderson, J. J. (1992). Weight loss reduces the risk for symptomatic knee osteoarthritis in women. The Framingham Study. *Annals of Internal Medicene, 116*(7), 535-539.

Ferguson, V. L., Ayers, R. A., Bateman, T. A., & Simske, S. J. (2003). Bone development and age-related bone loss in male C57BL/6J mice. *Bone, 33*(3), 387–398.

Findlay, D. M. (2007). Vascular pathology and osteoarthritis. *Rheumatology, 46*(12), 1763-1768.

Fitzpatrick, L. A. (2002). Secondary causes of osteoporosis. *Mayo Clinic Proceedings, 77*(5), 453-468.

Florencio-Silva, R., da Silva Sasso, G. R., Sasso-Cerri, E., Simões, M. J., & Cerri, P. S. (2015). Biology of Bone Tissue: Structure, Function, and Factors That Influence Bone Cells. *Biomed Research International, 2015*, 1-17.

Fox, J. C., & Keaveny, M. T. (2001). Trabecular Eccentricity and Bone Adaptation. *The Journal of Theoretical Biology, 212*, 211-221.

Fox, K. M., Magaziner, J., Hawkes, W. G., Yu-Yahiro, J., Hebel, J. R., Zimmerman, S. I., . . . Michael, R. (2000). Loss of Bone Density and Lean Body Mass after Hip Fracture. *Osteoporosis International, 11*(1), 31-35.

Frost, H. M. (1987). Bone "mass" and the "mechanostat": a proposal. *The Anatomical Record, 219*(1), 1-9.

Frost, H. M. (1990). Skeletal structural adaptations to mechanical usage (SATMU): 2. Redefining Wolff's Law: The remodeling problem. *The Anatomical Record, 226*(4), 414–422.

Frost, H. M. (2004). A 2003 Update of Bone Physiology and Wolff's Law for Clinicians. *The Angle Orthodontist, 74*(1), 3-15.

Galea, G. L., Hannuna, S., Meakin, L. B., Delisser, P. J., Lanyon, L. E., & Price, J. S. (2015). Quantification of Alterations in Cortical Bone Geometry Using Site Specificity Software in Mouse models of Aging and the Responses to Ovariectomy and Altered Loading. *Frontiers in Endocrinology, 26,* 52.

Gardinier, J. D., Al-Omaishi, S., Morris, M. D., & Kohn, D. H. (2016). PTH signaling mediates perilacunar remodeling during exercise. *Matrix Biology, 52-54,* 162–175.

Gerbaix, M., Vico, L., Ferrari, S. L., & Bonnet, N. (2015). Periostin expression contributes to cortical bone loss during unloading. *Bone, 71,* 94–100.

Globus, R. K., Bikle, D. D., & Morey-Holton, E. (1986). The Temporal Response of Bone to Unloading. *Endocrinology, 118,* 733–742.

Glyn-Jones, S., Palmer, A. J., Agricola, R., Price, A. J., & Vincent, T. L. (2015). Osteoarthritis. *Lancet, 386*(9991), 376-387.

Goldman, H. M., Hampson, N. A., Guth, J. J., Lin, D., & Jepsen, K. J. (2014). Intracortical remodeling parameters are associated with measures of bone robustness. *Anatomical Record, 297*(10), 1817–1828.

Goto, T., Yamaza, T., & Tanaka, T. (2003). Cathepsins in the osteoclast. *Journal of Electron Microscopy, 52*(6), 551-8.

Gross, T. S., & Rubin, C. T. (1995). Uniformity of resorptive bone loss induced by disuse. *Journal of Orthopaedic Research, 13*(5), 708–714.

Grynpas, M. D., Kasra, M., Renlund, R., & Pritzker, K. P. (1995). The effect of pamidronate in a new model of immobilization in the dog. *Bone, 17*(4), S225–S232.

Günther, K.-P., Stürmer, T., & Brenner, H. (2000). Obesity, overweight and patterns of osteoarthritis: the Ulm Osteoarthritis Study. *Journal of Clinical Epidemiology, 53*(3), 307-313.

Hadjidakis, D. J., & Androulakis, I. I. (2006). Bone remodeling. *Annals of the New York Academy of Sciences, 1092,* 385-96.

Halloran, B. P., Bikle, D. D., Cone, C. M., & Morey-Holton, E. (1988). Glucocorticoids and inhibition of bone formation induced by skeletal unloading. *The American Journal of Physiology, 255*(6), E875-9.

Hammond, M. A., Berman, A. G., Pacheco-Costa, R., Davis, H. M., Plotkin, L. I., & Wallace, J. M. (2016). Removing or truncating connexin 43 in murine osteocytes alters cortical geometry, nanoscale morphology, and tissue mechanics in the tibia. *Bone, 88*, 85–91.

He, G., & Ming, Z. (2010). A Computational Model for Cortical Endosteal Surface Remodeling Induced by Mechanical Disuse. *Mollecular and Cellular Biomechanics, 7*(1), 1-11.

He, G., Ming , Z., Hao, Z., Dong, Z., & Lin, Y. (2006). Theoretical analysis of contributions of disuse, basic multicellular unit activation threshold, and osteoblastic formation threshold to changes in bone mineral density at menopause. *Journal of Bone and Mineral Metabolism, 24*(5), 386-394.

Henriksen, K., Andreassen, K. V., Thudium, C. S., Gudmann, K. N., Moscatelli, I., Crüger-Hansen, C. E., . . . Neutzsky-Wulff, A. V. (2012). A specific subtype of osteoclasts secretes factors inducing nodule formation by osteoblasts. *Bone, 51*(3), 353-361.

Hofbauer, L. C., Lacey, D. L., Dunstan, C. R., Spelsberg, T. C., Riggs, B. L., & Khosla, S. (1999). Interleukin-1β and tumor necrosis factor-α, but not interleukin-6, stimulate osteoprotegerin ligand gene expression in human osteoblastic cells. *Bone, 25*(3), 255–259.

Horisberger, M., Fortuna, R., Valderrabano, V., & Herzog, W. (2013). Long-term repetitive mechanical loading of the knee joint by in vivo muscle stimulation accelerates cartilage degeneration and increases chondrocyte death in a rabbit model. *Clinical Biomechanics*, 536–543.

Ishijima, M., Rittling, S. R., Yamashita, T., Tsuji, K., Kurosawa, H., Nifuji, A., . . . Noda, M. (2001). Enhancement of Osteoclastic Bone Resorption and Suppression of Osteoblastic Bone Formation in Response to Reduced Mechanical Stress Do Not Occur in the Absence of Osteopontin. *The Journal of Experimental Medicene, 193*(3), 399-404.

Izawa, Y., Makita, T., Hino, S., Hashimoto, Y., Kushida, K., Inoue, T., & Orimo, H. (1981). Immobilization osteoporosis and active vitamin D: Effect of active vitamin D analogs on the

development of immobilization osteoporosis in rats. *Calcified Tissue International, 33*(1), 623-630.

Jabbar, S., Drury, J., Fordham, J. N., Datta, H. K., Francis, R. M., & Tuck, S. P. (2011). Osteoprotegerin, RANKL and bone turnover in postmenopausal osteoporosis. *Journal of Clinical Pathology, 64*(4), 354-7.

Jahani, M., Genever, P. G., Patton, R. J., Ahwal, F., & Fagan, M. J. (2012). The effect of osteocyte apoptosis on signalling in the osteocyte and bone lining cell network: a computer simulation. *Journal of Biomechanics, 45*(16), 2876–2883.

Janckila, A. J., Takahashi, K., Sun, S. Z., & Yam, L. T. (2001). Tartrate-resistant Acid Phosphatase Isoform 5b as Serum Marker for Osteoclastic Activity. *Clinical Chemistry, 47*(1), 74-80.

Jiang, S. D., Jiang, L. S., & Dai, L. Y. (2006). Mechanisms of osteoporosis in spinal cord injury. *Clinical Endocrinology, 65*(5), 555-565.

Jilka, R. L., Weinstein, R. S., Bellido, T., Roberson, P., Parfitt, A. M., & Manolagas, S. C. (1999). Increased bone formation by prevention of osteoblast apoptosis with parathyroid hormone. *The JOurnal of Clinnical Investigation, 104*(4), 439-446.

Jordan, G. R., Loveridge, N., Bell, K. L., Power, J., Rushton, N., & Reeve, J. (2000). Spatial clustering of remodeling osteons in the femoral neck cortex: a cause of weakness in hip fracture? *Bone, 26*(3), 305–313.

Jorgenson, B. L., Buie, H. R., McErlain, D. D., Sandino, C., & Boyd, S. K. (2015). A comparison of methods for in vivo assessment of cortical porosity in the human appendicular skeleton. *Bone, 73*, 167–175.

Kanis, J. A., Melton III, L. J., Christiansen, C., Johnston, C. C., & Khaltaev, N. (1994). The diagnosis of osteoporosis. *Journal of Bone and Mineral Research, 9*(8), 1137-1141.

Katsuyama, T., Fumio, O., Tomohiro, T., Inagaki, K., Takano-Narazaki, M., Matsumoto, Y., . . . Makino, H. (2015). Regulatory effects of fibroblast growth factor-8 and tumor necrosis factor-α on osteoblast marker expression induced by bone morphogenetic protein-2. *Peptides, 73*, 88–94.

Kawano, S., Kambe, F., Ohmori, S., Kanda, K., Nagaya, T., & Seo, H. (2001). Changes in mRNA levels of alkaline phosphatase and tartrate-resistant acid phosphatase in femur of ovariectomized rats: effects of estrogen and unloading. *Environmental Medicine, 45*(2), 55-7.

Kazakia, G. J., Tjong, W., Nirody, J. A., Burghardt, A. J., Carballido-Gamio, J., Patsch, J. M., . . . Ma, C. B. (2014). The influence of disuse on bone microstructure and mechanics assessed by HR-pQCT. *Bone, 63*, 132–140.

Kennedy, O. D., Brennan, O., Mauer, P., Rackard, S. M., O'Brien, F. J., Taylor, D., & Lee, T. C. (2008). The effects of increased intracortical remodeling on microcrack behaviour in compact bone. *Bone, 43*(5), 889–893.

Kenny, T. (2014, 04 03). *Osteoporosis*. Retrieved from Patient: http://www.patient.co.uk/health/osteoporosis-leaflet

Khurana, I. (2014). *Medical Physiology for Undergraduate Students* (2 ed.). Elsevier Health Sciences.

Klein-Nulend, J., Bacabac, R., & Mullender, M. (2005). Mechanobiology of bone tissue. *Pathologie Biologie, 53*, 576-580.

Kogianni, G., Mann, V., & Noble, B. S. (2008). Apoptotic Bodies Convey Activity Capable of Initiating Osteoclastogenesis and Localized Bone Destruction. *Journal of Bone and Mineral Research, 23*(6), 915–927.

Korpi-Steiner, N., Milhorn, D., & Hammett-Stabler, C. (2014). Osteoporosis in men. *Clinical Biochemistry, 47*(10-11), 950-959.

Kostenuik, P. J., Halloran, B. P., Morey-Holton, E. R., & Bikle, D. D. (1997). Skeletal unloading inhibits the in vitro proliferation and differentiation of rat osteoprogenitor cells. *American Journal of Physiology - Endocrinology and Metabolism, 273*(6), E1133-E1139.

Kulkarni, R. N., Bakker, A. D., Everts, V., & Klein-Nulend, J. (2012). Mechanical loading prevents the stimulating effect of IL-1β on osteocyte-modulated osteoclastogenesis. *Biochemical and Biophysical Research Communications, 420*(1), 11–16.

Kurata, K., Heino, T. J., Higaki, H., & Väänänen, H. K. (2006). Bone Marrow Cell Differentiation Induced by Mechanically Damaged Osteocytes in 3D Gel-Embedded Culture. *Journal of Bone and Mineral Research, 21*(4), 616–625.

Kusano, K., Miyaura, C., Inada, M., Tamura, T., Ito, A., Nagase, H., . . . Suda, T. (1997). Regulation of Matrix Metalloproteinases (MMP-2, -3, -9, and -13) by Interleukin-1 and Interleukin-6 in Mouse Calvaria: Association of MMP Induction with Bone Resorption. *Endocrinology, 139*(3), 1338-1345.

Lanyon, L. E., Magee, P. T., & Baggott, D. G. (1979). The relationship of functional stress and strain to the processes of bone remodeling. An experimental study on the sheep radius. *Journal of Biomechanics, 12*(8), 593-600.

Lean, J. M., Mackay, A. G., Chow, J. M., & Chambers, T. J. (1996). Osteocytic expression of mRNA for c-fos and IGF-I: An immediate early gene response to an osteogenic stimulus. *American Journal of Physiology - Endocrinology and Metabolism, 270*(6), E937-E945.

Leblanc, A. D., Schneider, V. S., Evans, H. J., Engelbretson, D. A., & Krebs, J. M. (1990). Bone mineral loss and recovery after 17 weeks of bed rest. *Journal of Bone and Mineral Research, 5*(8), 843–850.

Lindsay, R., Hart, D. M., Purdie, D., Ferguson, M. M., Clark, A. S., & Kraszewski, A. (1978). Comparative Effects of Oestrogen and a Progestogen on Bone Loss in Postmenopausal Women. *Clinical Science and Molecular Medicene, 54*(2), 193-195.

Linkhart, T. A., & Mohan, S. (1989). Parathyroid Hormone Stimulates Release of Insulin-Like Growth Factor-I (IGF-I) and IGF-II from Neonatal Mouse Calvaria in Organ Culture. *Endrocrinology, 125*(3).

Litwic, A., & Dennison, E. (2014, 10 10). *Osteoporosis in RA*. Retrieved 06 28, 2016, from National Rheumatoid Arthritis Society: http://www.nras.org.uk/osteoporosis-in-ra

LoCascio, V., Bonucci, E., Imbimbo, B., Ballanti, P., Adami, S., Milani, S., . . . DellaRocca, C. (1990). Bone loss in response to long-term glucocorticoid therapy. *Bone, 8*(1), 39-51.

Loveridge, N. (2004). *Spatial clustering of cortical remodeling and the temporal effects of reduced mechanical loading on bone micro-architecture.* Cambridge.

Loveridge, N., Power, J., Reeve, J., Warren, M., Doube, M., & Goodship, A. (2011). The ovine calcaneus: a useful model for fragility fractures of the hip? *2011 joint meeting of the Bone Research Society & the British Orthopaedic Research Society.* Cambridge: Frontiers Media S.A.

Lueken, S. A., Arnaud, S. B., Taylor, D. K., & Baylink, D. J. (1993). Changes in markers of bone formation and resorption in a bed rest model of weightlessness. *Journal of Bone and Mineral Research, 8*(12), 1433–1438.

Magnusson, H., Lindén, C., Karlsson, C., Obrant, K. J., & Karlsson, M. K. (2001). Exercise May Induce Reversible Low Bone Mass in Unloaded and High Bone Mass in Weight-Loaded Skeletal Regions. *Osteoporosis International, 12*(11), 950-955.

Martínez-Reina, J., Reina, I., Domínguez, J., & García-Aznar, J. M. (2014). A bone remodeling model including the effect of damage on the steering of BMUs. *Journal of the Mechanical Behavior of Biomedical Materials, 32*, 99–112.

Martini, F., Nath, J. L., & Bartholomew, E. F. (2014). Bones are classified according to shape and structure, and they have a variety of surface markings. In F. Martini, J. L. Nath, & E. F. Bartholomew, *Fundamentals of anatomy & physiology* (10th ed., pp. 206-207). Pearson.

Matsumoto, T., Nakayama, K., Kodama, Y., Fuse, H., Nakamura, T., & Fukumoto, S. (1998). Effect of Mechanical Unloading and Reloading on Periosteal Bone Formation and Gene Expression in Tail-Suspended Rapidly Growing Rats. *Bone, 22*(5), 89S–93S.

Mayhew, P. M., Thomas, C. D., Clement, J. G., Loveridge, N., Beck, T. J., Bonfield, W., . . . Reeve, J. (2005). Relation between age, femoral neck cortical stability, and hip fracture risk. *The Lancet, 366*(9480), 129–135.

Melton, J. L. (2001). The Prevalence of Osteoporosis: Gender and Racial Comparison. *Calcified Tissue International, 69*(4), 179-181.

Melton, L., Chrischilles, E. A., Cooper, C., Lane, A. W., & Riggs, B. L. (1992). Perspective. How many women have osteoporosis? *Journal of Bone and Mineral Research, 7*(9), 1005-10.

Mercuri, E. F., Daniel, A. L., Hecke, M. B., & Carvalho, L. (2016). Influence of different mechanical stimuli in a multi-scale mechanobiological isotropic model for bone remodeling. *Medical Engineering and Physics*. doi:10.1016/j.medengphy.2016.04.018

Mohan, S., & Baylink, D. J. (1995). Insulin-like growth factor system components and the coupling of bone formation to resorption. *Hormone Research, 45 Suppl 1*(59), 59-62.

Moonga, B. S., Moss, D. W., Patchell, A., & Zaidi, M. (1990). Intracellular regulation of enzyme secretion from rat osteoclasts and evidence for a functional role in bone resorption. *The Journal of Physiology, 429*(1), 29-45.

Morko, J., Kiviranta, R., Mulari, M. T., Ivaska, K. K., Väänänen, H. K., Vuorio, E., & Laitala-Leinonen, T. (2009). Overexpression of cathepsin K accelerates the resorption cycle and osteoblast differentiation in vitro. *Bone, 44*(4), 717–728.

Mosekilde, L. (1990). Consequences of the remodeling process for vertebral trabecular bone structure: a scanning electron microscopy study (uncoupling of unloaded structures). *Bone and Mineral, 10*(1), 13-35.

Munk-Jensen, N., Nielsen, S. P., Obel, E. B., & Eriksen, P. B. (1988). Reversal of postmenopausal vertebral bone loss by oestrogen and progestogen: a double blind placebo controlled study. *British Medical Journal, 296*, 1150-1152.

Nabavi, N., Khandani, A., Camirand, A., & Harrison, R. E. (2011). Effects of microgravity on osteoclast bone resorption and osteoblast cytoskeletal organization and adhesion. *Bone, 49*(5), 965–974.

Narra, N., Viik, J., Hyttinen, J., & Sievänen, H. (2013). Femoral neck cross-sectional geometry and exercise loading. *Clinical Physiology and Functional Imaging, 33*(4), 258–266.

Neer, R. M., Arnaud, C. D., Zanchetta, J. R., Prince, R., Gaich, G. A., Reginster, J.-Y., . . . Mitlak, B. H. (2001). Effect of Parathyroid Hormone (1-34) on Fractures and Bone Mineral Density in Postmenopausal Women with Osteoporosis. *The New England Journal of Medicene, 344*, 1434-1441.

Noble, B. S., Peet, N., Stevens, H. Y., Brabbs, A., Mosley, J. R., Reilly, G. C., . . . Lanyon, L. E. (2003). Mechanical loading: biphasic osteocyte survival and targeting of osteoclasts for bone destruction in rat cortical bone. *American Journal of Physiology - Cell Physiology, 284*(4), C934-C943.

Nobuhito, N., Shogo, K., Tomoka, H., Wataru, Y., Atsushi, M., & Koichi, M. (2016). Osteocyte-directed bone demineralization along canaliculi. *Bone, 84*, 279–288.

O'Brien, C. A., Jia, D., Plotkin, L. I., Bellido, T., Powers, C. C., Stewart, S. A., . . . Weinstein, R. S. (2003). Glucocorticoids Act Directly on Osteoblasts and Osteocytes to Induce Their Apoptosis and Reduce Bone Formation and Strength. *Endocrinology, 145*(4), 1835–1841.

Oddie, G. W., Schenk, G., Angel, N. Z., Walsh, N., Guddat, L. W., De Jersey, J., . . . Hume, D. A. (2000). Structure, Function, and Regulation of Tartrate-Resistant Acid Phosphatase. *Bone, 27*(5), 575-584.

Oddie, G. W., Schenk, G., Angel, N. Z., Walsh, N., Guddat, L. W., de Jersey, J., . . . Hume, D. A. (2000). Structure, function, and regulation of tartrate-resistant acid phosphatase. *Bone, 27*(5), 575–584.

O'Flaherty, E. J. (2000). Modeling Normal Aging Bone Loss, with Consideration of Bone Loss in Osteoporosis. *Toxicological Sciences*, 171-188.

Ohuchi, E., Imai, K., Fujii, Y., Sato, H., Seiki, M., & Okada, Y. (1997). Membrane Type 1 Matrix Metalloproteinase Digests Interstitial Collagens and Other Extracellular Matrix Macromolecules. *The Jounral of Biological Chemistry, 272*(4), 2446–2451.

Plotkin, L. I., Rodriguez de Gortazar, A., Davis, H. M., Condon, K. W., Gabilondo, H., Maycas, M., . . . Bellido, T. (2015). Inhibition of Osteocyte Apoptosis Prevents the Increase in Osteocytic RANKL but it does not Stop Bone Resorption or the Loss of Bone Induced by Unloading. *The Journal of Biological Chemistry, 291*, 1538.

Plotkin, L. I., Weinstein, R. S., Parfitt, A. M., Roberson, P. K., Manolagas, S. C., & Bellido, T. (1999). Prevention of osteocyte and osteoblast apoptosis by bisphosphonates and calcitonin. *The Journal of Clinical Investigation, 104*(10), 1363–1374.

Power, J., Loveridge, N., Lyon, A., Rushton, N., Parker, M., & Reeve, J. (2003). Bone Remodeling at the Endocortical Surface of the Human Femoral Neck. *Journal of Bone and Mineral Research*, 1775-1780.

Power, J., Loveridge, N., Lyon, A., Rushton, N., Parker, M., & Reeve, J. (2003). Bone Remodeling at the Endocortical Surface of the Human Femoral Neck: A Mechanism for Regional Cortical Thinning in Cases of Hip Fracture. *Journal of Bone and Mineral Research, 18*(10), 1775–1780.

Qin, Y., Lam, H., Malbari, M., Shih, M., & Carroll, W. (2009). Inhibition of bone loss using dynamic muscle stimulation in a disuse osteopenia model. *Abstracts from the 2nd Joint Meeting of the International Bone & Mineral Society and the Australian & New Zealand Bone & Mineral Society. 44,* pp. S154–S155. Sydney: Elsevier.

Qiu, S., Fyhrie, D. P., Palnitkar, S., & Rao, D. S. (2003). Histomorphometric assessment of Haversian canal and osteocyte lacunae in different-sized osteons in human rib. *The Anatomical Record Part A: Discoveries in Molecular, Cellular, and Evolutionary Biology, 272A*(2), 520–525.

Qiu, S., Rao, D. S., Fyhrie, D. P., Palnitkar, S., & Parfitt, A. M. (2005). The morphological association between microcracks and osteocyte lacunae in human cortical bone. *Bone, 37*(1), 10–15.

Raisz, L., Bilezikian, J., & Martin, T. (2008). *Pathophysiology of osteoporosis* (Vol. 2). Elsevier.

Rana, T., Schultz, M. A., Freeman, M. L., & Biswas, S. (2012). Loss of Nrf2 accelerates ionizing radiation-induced bone loss by upregulating RANKL. *Free Radical Biology and Medicine, 53*(12), 2298–2307.

Reinhold, E. G. (2015). Hypothesis: Coupling between Resorption and Formation in Cancellous bone Remodeling is a Mechanically Controlled Event. *Frontiers in Endocrinology (Lausanne), 6*(82).

Riggs, B. L., Melton III, L. J., Robb, R. A., Camp, J. J., Atkinson, E. J., Peterson, J. M., . . . Khosla, S. (2004). Population-Based Study of Age and Sex Differences in Bone Volumetric Density, Size, Geometry, and Structure at Different Skeletal Sites. *Journal of Bone and Mineral Research, 19*(12), 1945–1954.

Riis, B., Hansen, M. A., Jensen, A. M., Overgaard, K., & Christiansen, C. (1996). Low bone mass and fast rate of bone loss at menopause: Equal risk factors for future fracture: A 15-year follow-up Study. *Bone, 19*(1), 9–12.

Rizzo, D. C. (2015). The Function of the Skeletal System. In D. C. Rizzo, *Fundamentals of Anatomy and Physiology* (4th ed., pp. 138-139). Cengage Learning.

Rucci, N. (2008). Molecular biology of bone remodeling. *Clinical Cases Mineral and Bone Metabolism, 5*(1), 49–56.

Russo, C. R., Lauretani, F., Seeman, E., Bartali, B., Bandinelli, S., Di Iorio, A., . . . Ferrucci, L. (2006). Structural adaptations to bone loss in aging men and women. *Bone, 38*(1), 112–118.

Sakai, A., & Nakamura, T. (2001). Changes in Trabecular Bone Cell Marrow Development in Tail-suspended Mice. *Journal of Musculoskeletal and Neuronal Interactions, 1*(4), 387-392.

Schett, G., & Teitelbaum, S. L. (2009). Osteoclasts and Arthritis. *Journal of Bone and Mineral Research, 24*(7), 1142–1146.

Schneider, D. L., Barrett-Connor, E. L., & Morton, D. J. (1997). Timing of Postmenopausal Estrogen for Optimal Bone Mineral Density: The Rancho Bernardo Study. *The Journal of the American Medical Association, 277*(7), 543-547.

Sheu, T.-J., Schwarz, E. M., Martinez, D. A., O'Keefe, R. J., Rosier, R. N., Zuscik, M. J., & Puzas, J. E. (2003). A Phage Display Technique Identifies a Novel Regulator of Cell Differentiation. *The Journal of Biological Chemistry, 278*, 438-443.

Sims, N. A., & Martin, T. J. (2014). Coupling the activities of bone formation and resorption: a multitude of signals within the basic multicellular unit. *BoneKEy Reports, 3*, 481.

Siwapituk, W., & Kitisomprayoonkul, W. (2016). Bone turnover increases during supervised treadmill walking in Thai postmenopausal women. *Osteoporosis and Sarcopenia, 2*(1), 41–44.

Skedros, J. G., Mason, M. W., & Bloebaum, R. D. (1994). Differences in osteonal micromorphology between tensile and compressive cortices of a bending skeletal system: Indications of potential strain-specific differences in bone microstructure. *The Anatomical Record, 239*(4), 405–413.

Skedros, J. G., Mason, M. W., & Bloebaum, R. D. (2001). Modeling and remodeling in a developing artiodactyl calcaneus: A model for evaluating Frost's Mechanostat hypothesis and its corollaries. *The Anatomical Record, 263*(2), 167–185.

Skedros, J. G., Mendenhall, S. D., Kiser, C. J., & Winet, H. (2009). Interpreting cortical bone adaptation and load history by quantifying osteon morphotypes in circularly polarized light images. *Bone, 44*(3), 392-403.

Skerry, T. M., & Lanyon, L. E. (1995). Interruption of disuse by short duration walking exercise does not prevent bone loss in the sheep calcaneus. *Bone, 16*(2), 269–274.

Smith, S. M., Wastney, M. E., O'Brien, K. O., Morukov, B. V., Larina, I. M., Abrams, S. A., . . . Shackelford, L. C. (2005). Bone markers, calcium metabolism, and calcium kinetics during extended-duration space flight on the Mir Space Station. *Journal of Bone and Mineral Research, 20*(2), 208-218.

Solberg, L. B., Stang, E., Brorson, S. H., Andersson, G., & Reinholt, F. P. (2014). Tartrate-resistant acid phosphatase (TRAP) co-localizes with receptor activator of NF-KB ligand (RANKL) and osteoprotegerin (OPG) in lysosomal-associated membrane protein 1 (LAMP1)-positive vesicles in rat osteoblasts and osteocytes. *Histochemistry and Cell Biology, 143*, 195–207.

Sugawara, Y., Kamioka, H., Ishihara, Y., Fujisawa, N., Kawanabe, N., & Yamashiro, T. (2013). The early mouse 3D osteocyte network in the presence and absence of mechanical loading. *Bone, 52*(1), 189–196.

Sun, S., Karsdal, M. A., Bay-Jensen, A. C., Sørensen, M. G., Zheng, Q., Dziegiel, M. H., . . . Henriksen, K. (2013). The development and characterization of an ELISA specifically detecting the active form of cathepsin K. *Clinical Biochemistry, 46*(15), 1601–1606.

Tamura, T., Udagawa, N., Takahashi, N., Miyaura, C., Tanaka, S., Yamada, Y., . . . Taga, T. (1993). Soluble interleukin-6 receptor triggers osteoclast formation by interleukin 6. *Proceedings of the National Academy of Sciences of the United States of America, 90*(24), 11924–11928.

Tannenbaum, C., Clark, J., Schwartzman, K., Wallenstein, S., Lapinski, R., Meier, D., & Luckey, M. (2002). Yield of Laboratory Testing of Identify Secondary Contibutors to Osteoporosis in Otherwise Healthy Women. *The Journal of Clinical Endocrinology & Metabolism, 87*(10), 4431-4437.

Taylor, A. F., Saunders, M. M., Shingle, D. L., Cimbala, J. M., Zhou, Z., & Donahue, H. J. (2007). Mechanically stimulated osteocytes regulate osteoblastic activity via gap junctions. *American Journal of Physiology*, C545-C552.

Thomas, C. L., Feik, S. A., & Clement, J. G. (2006). Increase in pore area, and not pore density, is the main determinant in the development of porosity in human cortical bone. *Journal of Anatomy, 209*(2), 219–230.

Thomas, T., Skerry, T. M., Vico, L., Caulin, F., Lanyon, L. E., & Alexandre, C. (1995). Ineffectiveness of calcitonin on a local-disuse osteoporosis in the sheep: A histomorphometric study. *Calcified Tissue International, 57*(3), 224-228.

Thomas, T., Vico, L., Skerry, T. M., Caulin, F., Lanyon, L. E., Alexandre, C., & Lafage, M. H. (1996). Architectural modifications and cellular response during disuse-related bone loss in calcaneus of the sheep. *Journal of Applied Physiology, 80*(1), 198-202.

Thomsen, J. S., Christensen, L. L., Jens Bay Vegger, J. B., & Nyengaard, J. R. (2012). Loss of Bone Strength is Dependent on Skeletal Site in Disuse Osteoporosis in Rats. *Calcified Tissue International, 90*(1), 294–306.

Tonino, A. J., Davidson, C. L., Klopper, P. J., & Linclau, L. A. (1973). Protection from stress in bone and its effects. Experiments with stainless steel and plastic plates in dogs. *The Bone & Joint Journal, 58-B*(1), 107-113.

Troen, B. R. (2004). The Role of Cathepsin K in Normal Bone Resorption. *Drug News & Perspectives, 17*(1), 19.

Tsuboi, M., Kawakami, A., Nakashima, T., Matsuoka, N., Urayama, S., Kawabe, Y., . . . Eguchi, K. (1999). Tumor necrosis factor-α and interleukin-1β increase the Fas-mediated apoptosis of human osteoblasts. *Journal of Laboratory and Clinical Medicine, 134*(3), 222–231.

Turner, C. H. (1998). Three rules for bone adaptation to mechanical stimuli. *Bone, 23*(5), 399–407.

Tyrovola, J. B., & Odont, X. X. (2015). The "Mechanostat Theory" of Frost and the OPG/RANKL/RANK System. *Journal of Cellular Biochemistry, 116*(12), 2724–2729.

van Lenthe, G. H., Hagenmüller, H., Bohner, M., Hollister, S. J., Meinel, L., & Müller, R. (2007). Nondestructive micro-computed tomography for biological imaging and quantification of scaffold–bone interaction in vivo. *Biomaterials, 28*(15), 2479–2490.

van Staa, T. P., Dennison, E. M., Leufkens, H. M., & Cooper, C. (2001). Epidemiology of fractures in England and Wales. *Bone*, 517–522.

Van Staa, T. P., Leufkens, H. G., Abenhaim, L., Zhang, B., & Cooper, C. (2000). Use of Oral Corticosteroids and Risk of Fractures. *Journal of Bone and Mineral Research, 15*(6), 993–1000.

Vashishth, D., Verborgt, O., Divine, G., Schaffler, M. B., & Fyhrie, D. P. (2000). Decline in osteocyte lacunar density in human cortical bone is associated with accumulation of microcracks with age. *Bone, 26*(4), 375–380.

Verborgt, O., Gibson, G. J., & Schaffler, M. B. (2000). Loss of osteocyte integrity in association with microdamage and bone remodeling after fatigue in vivo. *Journal of Bone and Mineral Research, 15*(1), 60–67.

Vico, L., Novikov, V. E., Very, J. M., & Alexandre, C. (1991). Bone histomorphometric comparison of rat tibial metaphysis after 7-day tail suspension vs. 7-day spaceflight. *Aviation, space and environmental medicene, 62*(1), 26-31.

Vigorita, V. J. (1999). *Orthopaedic Pathology* (2 ed.). Philadelphia: Lippincott, Williams & Wilkins.

Vilayphiou, N., Boutroy, S., Sornay-Rendu, E., Van Rietbergen, B., & Chapurlat, R. (2016). Age-related changes in bone strength from HR-pQCT derived microarchitectural parameters with an emphasis on the role of cortical porosity. *Bone, 83*, 233–240.

Wang, Y. (2015). An Investigation of Human Cortical Bone's Response to Mechanical Stimuli. *Procedia Technology* (pp. 60-65). Geelong: Elsevier.

Weiner, S. (1986). Organization of hydroxyapatite crystals within collagen fibrils. *FEBS Letters, 206*(2), 185–366.

Weinreb, M., Rodan, G. A., & Thompson, D. D. (1989). Osteopenia in the immobilized rat hind limb is associated with increased bone resorption and decreased bone formation. *Bone, 10*(3), 187-194.

Woolf, A. D., & Pfleger, B. (2003). Burden of major musculoskeletal conditions. *Bulletin of the World Health Organization, 81*(9), 646-56.

World Health Organization. (2004). *WHO Scientific Group on the Assessment of Osteoporosis at Primary Health Care Level.* Brussels: World Health Organization.

Wronski, T. J., & Morey, E. R. (1982). Skeletal abnormalities in rats induced by simulated weightlessness. *Metabolic Bone Disease and Related Research, 4*(1), 69-75.

Xiong, J., & O'Brien, C. A. (2012). Osteocyte RANKL: New insights into the control of bone remodeling. *Journal of Bone and Mineral Research, 27*(3), 499–505.

Xiong, J., Piemontese, M., Thostenson, J. D., Weinstein, R. S., Manolagas, S. C., & O'Brien, C. A. (2014). Osteocyte-derived RANKL is a critical mediator of the increased bone resorption caused by dietary calcium deficiency. *Bone, 66*, 146–154.

Yang Li, C., Price, C., Delisser, K., Nasser, P., Laudier, D., Clement, M., . . . Schaffler, M. B. (2005). Long-Term Disuse Osteoporosis Seems Less Sensitive to Bisphosphonate Treatment Than Other Osteoporosis. *Journal of Bone and Mineral Research, 20*(1), 117–124.

Yerramshetty, J., & Akkus, O. (2012). *Skeletal Aging and Osteoporosis: Biomechanics and Mechanobiology.* (M. J. Silva, Ed.) Springer Science & Business Media.

Young, L. H., Youkyung, K., Jung , K. J., & In, G. J. (2015). Homeostasis-based aging model for trabecular changes and its correlation with age-matched bone mineral densities and radiographs. *European Journal of Radiology, 84*(11), 2261–2268.

Zaidi, M., Moonga, B., Moss, D. W., & MacIntyre, I. (1989). Inhibition of osteoclastic acid phosphatase abolishes bone resorption. *Biochemical and Biophysical Research Communications, 1*, 68–71.

Zanelli Joan, M., Pearson, J., Moyes, S. T., Green, J., Reeve, J., Garrahan, N. J., . . . Meunier, P. J. (1993). Methods for the histological study of femoral neck bone remodeling in patients with fractured neck of femur. *Bone, 14*(3), 249-255.

Zhang, Y.-H., Heulsmann, A., Tondravi, M. M., Mukherjee, A., & Abu-Amer, Y. (2001). Tumor Necrosis Factor-α (TNF) Stimulates RANKL-induced Osteoclastogenesis via Coupling of TNF Type 1 Receptor and RANK Signaling Pathways. *The Journal of Biological Chemistry, 276*, 563-568.

Zhao, L., Dodge, T., Ledet, E., & Yokota, H. (2011). Knee Loading Stimulates Bone Formation in Tail-Suspended Mouse Hindlimb. *Biological Sciences in Space, 25*(2-4), 77-82.

6.2.2: Appendix of raw data

6.2.21: Cortical Porosity Raw Data

Table 4: %porosity over all regions for each bone image at their respective time points

All Regions	
Time Stamp	%porosity
Day 0	
3494L	5.4
5146L	5.0
5157L	8.1
5183L	4.6
5307L	3.9
5311L	3.2
Mean	5.0
Week 4	
5147L	3.8
5151L	6.3
5164L	3.1
5194L	3.1
5199L	3.4
Mean	4.0
Week 16	
5076L	5.2
5087L	5.6
5088L	5.7
5106L	6.9
5132L	7.3
5196L	4.0
Mean	5.8

Table 5: %porosity of the medial region for each bone image at their respective time points

Medial	
Time Stamp	%porosity
Day 0	
3494L	8.4
5146L	4.7
5157L	5.1
5183L	5.7
5307L	2.8
5311L	2.4
Mean	4.9
Week 4	
5147L	2.5
5151L	2.3
5164L	5.7
5194L	2.6
5199L	4.3
Mean	3.5
Week 16	
5076L	2.4
5087L	7.0
5088L	2.5
5106L	6.0
5132L	4.3
5196L	5.1
Mean	4.6

Table 6: %porosity of the lateral region for each bone image at their respective time points

Lateral	
Time Stamp	%porosity
Day 0	
3494L	2.1
5146L	4.8
5157L	7.6
5183L	2.1
5307L	2.7
5311L	2.6
Mean	3.6
Week 4	
5147L	2.9
5151L	2.6
5164L	9.7
5194L	5.7
5199L	1.7
Mean	4.5
Week 16	
5076L	1.5
5087L	2.4
5088L	5.8
5106L	3.5
5132L	9.9
5196L	2.8
Mean	4.3

Table 7: %porosity of the ventral region for each bone image at their respective time points

Ventral	
Time Stamp	%porosity
Day 0	
3494L	5.4
5146L	7.9
5157L	16.2
5183L	6.0
5307L	7.5
5311L	6.1
Mean	8.2
Week 4	
5147L	3.3
5151L	4.2
5164L	6.2
5194L	2.0
5199L	2.6
Mean	3.7
Week 16	
5076L	10.6
5087L	11.4
5088L	8.7
5106L	5.9
5132L	13.1
5196L	5.0
Mean	9.1

Table 8: %porosity of the dorsal region for each bone image at their respective time points

Dorsal	
Time Stamp	%porosity
Day 0	
3494L	4.1
5146L	3.4
5157L	4.3
5183L	3.4
5307L	3.0
5311L	2.4
Mean	3.5
Week 4	
5147L	7.3
5151L	3.8
5164L	4.9
5194L	3.1
5199L	5.0
Mean	4.8
Week 16	
5076L	3.4
5087L	7.4
5088L	6.5
5106L	13.4
5132L	5.3
5196L	8.5
Mean	7.4

6.2.22 Cortical Width Raw Data

Table 9: Cortical width over all regions for each bone image at their respective time points

All Regions	
Time Stamp	Cortical Width (mm)
Day 0	
3494L	7.7
5146L	9.1
5157L	8.0
5183L	7.9
5307L	6.5
5311L	9.3
Mean	8.1
Week 4	
5147L	8.0
5151L	8.2
5194L	9.1
5199L	9.7
5164L	7.0
Mean	8.4
Week 16	
5076L	6.1
5087L	7.0
5088L	6.5
5106L	7.4
5132L	6.8
5196L	7.7
Mean	6.9

Table 10: Cortical width of the medial region for each bone image at their respective time points

Medial	
Time Stamp	Cortical Width (mm)
Day 0	
3494L	2.0
5146L	2.0
5157L	2.0
5183L	1.9
5307L	1.9
5311L	2.0
Mean	2.0
Week 4	
5147L	2.0
5151L	2.1
5194L	2.6
5199L	2.4
5164L	1.8
Mean	2.2
Week 16	
5076L	1.5
5087L	1.8
5088L	1.5
5106L	1.9
5132L	1.7
5196L	1.9
Mean	1.7

Table 11: Cortical width of the lateral region for each bone image at their respective time points

Lateral	
Time Stamp	Cortical Width (mm)
Day 0	
3494L	1.7
5146L	2.1
5157L	1.6
5183L	1.6
5307L	1.2
5311L	2.1
Mean	1.7
Week 4	
5147L	1.6
5151L	1.6
5194L	1.7
5199L	1.9
5164L	1.4
Mean	1.6
Week 16	
5076L	1.6
5087L	1.6
5088L	1.5
5106L	1.5
5132L	1.5
5196L	1.4
Mean	1.5

Table 12: Cortical width of the ventral region for each bone image at their respective time points

Ventral	
Time Stamp	Cortical Width (mm)
Day 0	
3494L	2.6
5146L	3.1
5157L	2.9
5183L	3.1
5307L	2.1
5311L	3.4
Mean	2.9
Week 4	
5147L	2.9
5151L	2.9
5194L	3.2
5199L	3.2
5164L	2.9
Mean	3.0
Week 16	
5076L	2.2
5087L	2.5
5088L	2.7
5106L	1.7
5132L	1.2
5196L	2.7
Mean	2.2

Table 13: Cortical width of the dorsal region for each bone image at their respective time points

Dorsal	
Time Stamp	Cortical Width (mm)
Day 0	
3494L	1.4
5146L	1.9
5157L	1.5
5183L	1.2
5307L	1.3
5311L	1.8
Mean	1.5
Week 4	
5147L	1.5
5151L	1.6
5194L	1.5
5199L	2.1
5164L	1.0
Mean	1.6
Week 16	
5076L	0.9
5087L	1.1
5088L	0.8
5106L	2.3
5132L	2.4
5196L	1.6
Mean	1.5

6.2.23 Forming Canal Raw Data

Table 14: % Forming canal over all regions for each bone image at their respective time points

Total Combined Regions	
Time Stamp	% of Forming Canals
Day 0	
3493L	4.18
5146L	1.34
5157L	2.96
5183L	3.34
5307L	16.14
5311L	4.86
Mean	5.47
Week 4	
5147L	3.03
5151L	3.55
5194L	4.89
5199L	5.42
5164L	1.35
Mean	3.65
Week 16	
5076L	4.61
5087L	20.59
5088L	7.25
5106L	4.34
5132L	8.22
5196L	8.36
Mean	8.90

Table 15: % Forming canals of the medial region for each bone image at their respective time points

Medial	
Time Stamp	% of Forming Canals
Day 0	
3493L	1.46
5146L	1.83
5157L	2.67
5183L	1.97
5307L	10.70
5311L	2.59
Mean	3.54
Week 4	
5147L	4.08
5151L	3.14
5194L	3.49
5199L	4.00
5164L	4.63
Mean	3.87
Week 16	
5076L	3.70
5087L	6.95
5088L	4.93
5106L	5.82
5132L	8.36
5196L	7.40
Mean	6.19

Table 16: % Forming canals of the lateral region for each bone image at their respective time points

Lateral	
Time Stamp	% of Forming Canals
Day 0	
3493L	4.25
5146L	1.65
5157L	4.84
5183L	6.74
5307L	44.62
5311L	7.58
Mean	11.61
Week 4	
5147L	3.17
5151L	5.07
5194L	8.42
5199L	8.79
5164L	4.57
Mean	6.00
Week 16	
5076L	8.54
5087L	10.05
5088L	10.85
5106L	5.09
5132L	9.84
5196L	13.79
Mean	9.69

Table 17: % Forming canals of the ventral region for each bone image at their respective time points

Ventral	
Time Stamp	% of Forming Canals
Day 0	
3493L	7.16
5146L	0.58
5157L	1.85
5183L	1.98
5307L	21.42
5311L	4.28
Mean	6.21
Week 4	
5147L	2.12
5151L	1.47
5194L	2.40
5199L	3.69
5164L	4.00
Mean	2.74
Week 16	
5076L	2.76
5087L	4.36
5088L	6.48
5106L	2.39
5132L	6.67
5196L	4.19
Mean	4.48

Table 18: % Forming canals of the dorsal region for each bone image at their respective time points

Dorsal	
Time Stamp	% of Forming Canals
Day 0	
3493L	7.90
5146L	1.83
5157L	4.07
5183L	3.98
5307L	9.27
5311L	7.20
Mean	5.71
Week 4	
5147L	2.43
5151L	5.79
5194L	8.19
5199L	6.96
5164L	5.88
Mean	5.85
Week 16	
5076L	3.82
5087L	8.98
5088L	7.76
5106L	7.14
5132L	8.47
5196L	12.05
Mean	8.04